Leveraging the Use of Liquid Metal Channels to Reconfigure Antennas' Impedance and Radiation Performance

by

Siddharth Kishore

A thesis presented to the Lakehead University in partial fulfillment of the required degree of

Master of Science in
Electrical and Computer Engineering

Faculty of Engineering
Lakehead University
Thunder Bay, Ontario Canada

April 2025

ABSTRACT

The advent of liquid metals in the domain of RF system has opened new avenues for the researchers in smart antenna designs. Reconfigurability of antenna's characteristics has been a keen topic of interest for the past several decades. Under this umbrella, various techniques have been employed by the designers to achieve the desired tunability. These include but are not limited to, use of varactor and p-i-n diodes, magnetic materials, ferroelectric materials, MEMS. Alongside these, embedding of metallic microfluidic channels within the antenna substrate has emerged as the most recent and novel technique. Metallic fluids, with their high conductivity and fluid nature, provide unique ideas to the designer. This thesis explores two different antenna designs that rely on EGaIn channels, a non-toxic metallic fluid, to achieve frequency switching and polarization reconfigurability. A circular patch antenna is designed at 2.5 GHz on a Rogers 5880 substrate with an integrated artificial magnetic conductor layer to boost its gain. Acrylic substrates have been used to realize EGaIn channels between the antenna and the ground plane. By optimizing the AMC for both the vacuum and metal-filled states, the design achieves efficient frequency switching from 2.5 GHz to 1.6 GHz with stable gain performance. This provides a proof-of-concept for how a switchable artificial magnetic conductor can be designed using such a technique. On the other hand, the second design validates polarization diversity with the application of EGaIn channels within the antenna substrate. A single patch antenna is shown to operate both with linear and circular polarizations using this concept at 2.5 GHz. Both the designs, i.e., polarization reconfigurable and frequency switchable, rely on microfluidic channels integrated into the acrylic substrates, allowing the antennas to switch between two or more operational

states. The research thus highlights the potential of microfluidic channels to achieve reconfigurability in modern antenna systems.

ACKNOWLEDGMENT

I would like to express my immense gratitude to Farhan Abdul Ghaffar, my supervisor, for providing me with the opportunity to work under his supervision. Your unwavering support, immense knowledge and constant encouragement have allowed me to elevate my research and has reinstated my passion for academia. Thank you for believing in me and providing a conducive environment where I could perform to the best of my abilities. This thesis would have been impossible without your insight and guidance.

I would also like to appreciate the examining committee, Dr. Yushi Zhou and Dr. Shafiqul Hai. Your positive feedback and comments have helped in improving the quality of this work.

I am grateful for my parents, Kishore and Vinitha. My love for you is immeasurable and I hope this makes you proud. I am also grateful for the immense support from all my friends throughout this journey. Finally, I would like to thank Shahinshah Ali for his help with simulations and CMC Microsystems for their support with the Ansys software.

TABLE OF CONTENTS

LIST OF FIGURES

LIST OF ABBREVIATIONS

CHAPTER 1: INTRODUCTION

1.1 Motivation

Antenna reconfigurability has always been a major area of interest for researchers and the current communication landscape has also led to an increased demand for such antenna systems. The versatility of antennas can be defined in terms of their frequency, polarization, radiation, etc., for different kinds of applications [1]. Among these, frequency reconfiguration has found a lot of application in the modern antenna system. The rationale is the presence of multiple channels to accommodate more devices at the same endpoint, for example on routers/repeaters. These channels are on two separate frequency bands, such as 2.4/5 GHz for Wi-Fi, and is achieved through frequency reconfiguration [2].

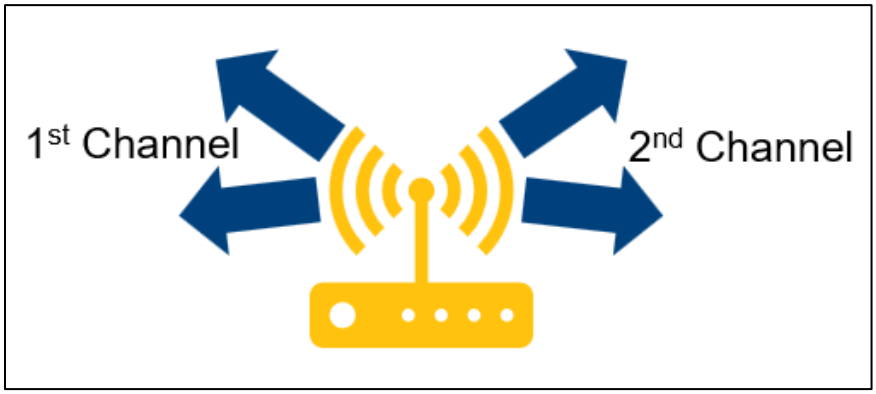

Fig. 1.1 Routers Using Frequency Reconfiguration

Likewise, another application of smart antenna systems is their beam steering or pattern reconfiguration capabilities. Many applications require the antenna's main beam to be actively redirected, a satellite in orbit for example, shown in Fig. 1.2 (a). This reconfiguration method is also used to reduce path loss, interference and increase gain [3]. Finally, at least for the context of this thesis, the third type of antenna reconfigurability

can be regarded as, polarization reconfiguration, an especially attractive quality in agile antenna systems. Antennas can radiate linear (LP), right-hand circular (RHCP) or left-hand circular polarization (LHCP) radiation, portrayed in Fig. 1.2 (b). For two antennas to communicate effectively, they should be polarization matched [1]. Thus, by reconfiguring antenna's polarization secured communication channel can be established that is immune to external probing. Thus, the above the 3 discussed herewith can be regarded as the basic types of antenna reconfiguration.

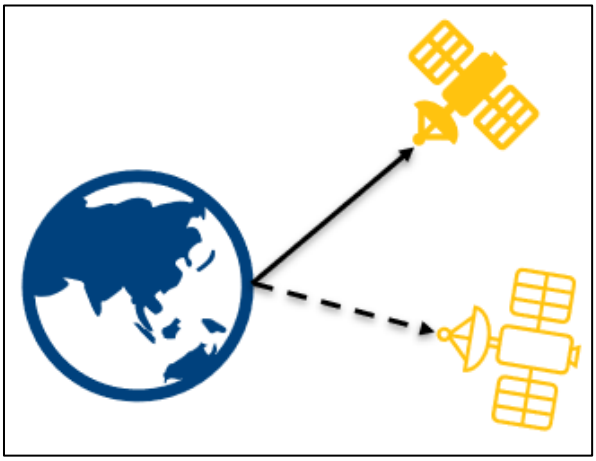

(a)

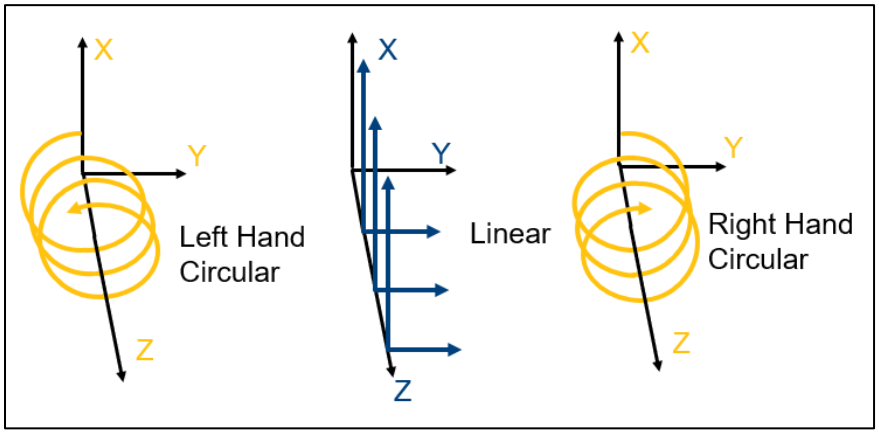

(b)

Fig. 1.2 (a) Satellites using Beam Steering (b) Different Types of Polarization

A quick glance at the literature shows that reconfigurability has been a deeply investigated subject and multiple methods have emerged and refined over the last few decades. Switches, varactor and p-i-n diodes are used to turn ON or OFF different elements of an antenna. For example, by changing the biasing of varactors and in turn their capacitances, antennas have been shown to achieve frequency [4], [5], [6], pattern [7], [8] and polarization reconfiguration [9], [10]. Micro-electromechanical systems (MEMS) have also acquired popularity from their small size and have been extensively employed to achieve the same effect [11], [12]. Similarly, ferromagnetic materials through their variable magnetic properties, can also be a good candidate for such applications [13], [14], [15], [16]. However, the topic of this thesis focusses on an entirely new idea i.e., microfluidic channels.

Metallic or microfluidic channels have recently garnered significant interest in the radio frequency (RF) community as a method to achieve antennas and circuit reconfiguration. Their metallic character offers high conductivity while their fluid nature allows for the creation of channels within a substrate where they can be injected as per the designer's choice. The metal thus flows through these channels and achieve intricate but effective structures. A combination of 75% Gallium and 25% Indium (EGaIn) has become the most widely used liquid metal (LM) with designs demonstrating different kinds of reconfiguration. Most designs use filling and emptying of channels as distinct states and use this process to achieve some reconfiguration. These articles demonstrate use of partially filled channels (with EGaIn), EGaIn integrated with the antenna surface, metasurfaces, and EGaIn as reflectors, among many other interesting methods. The fluid is also non-toxic, potentially providing an avenue for applications in wearable and

biomedical devices. While conventional methods of reconfiguration have lots of research dedicated to it along with decades of manufacturing refinement, the use of microfluidic metals is relatively new in the field of antenna reconfigurability. Thus, it can be regarded as a relatively greener area for researchers. Forming a reliable design procedure for integrating fluid metals along with understanding the manufacturing process is essential to deepening the field of reconfigurable antenna systems.

1.2 Thesis Objective

The objectives of this thesis can be summarized as follows,

- To demonstrate the use of metallic fluids/microfluidics in achieving antenna reconfiguration.
- To study the use of microfluidic channels as part of an Artificial Magnetic Conductor (AMC) layer to achieve gain enhancement
- To design a frequency-switchable antenna using liquid metal channels within the substrate that can operate at two working frequencies.
- To design a polarization reconfigurable antenna using the same technique as discussed above that can switch between linear and circular polarizations while maintaining impedance and radiation performance.

1.3 Thesis Contribution

Within the boundaries of the objectives outlined above, the contributions of this thesis can be detailed as follows,

- A frequency switching antenna system that achieves good impedance matching and decent radiation performance at two different frequencies.

- The antenna is designed to operate at 2.48 GHz to provide a gain of 7.5 dBi. This high gain is the result of integrating an active AMC layer between the antenna and the ground plane.
- The AMC layer is designed to be adaptable by injecting and removing the EGaIn liquid within the substrate channels. This process provides for the switching of frequency from 2.48 GHz to 1.65 GHz while providing acceptable matching and gain conditions.

- The second contribution pertains to the design of a polarization agile antenna system that can switch between linear and circular polarization states at the frequency of 2.5 GHz.
  - Again, the design methodology of this antenna is consistent with the previous one where the active design element is the EGaIn channel.
  - The antenna achieves a significant change in axial ratio, with the linear state showing a value of 9 dB that drops to 2 dB for RHCP and 3 dB for LHCP states.
  - Throughout this process, the gain and the impedance of the antenna remain stable to show consistent operation at the center frequency of 2.5 GHz.

1.4 Thesis Organisation

Chapter 2 provides a brief background on fluid metals and the use of EGaIn within antenna systems. A literature review of existing designs is provided, with an emphasis on reconfigurable designs. The fabrication process of the few designs is also presented in this chapter to give an idea to the readers about the challenges that could be encountered during the realization of such systems.

Chapter 3 outlined the design process of the frequency reconfigurable antenna. The parametric analysis performed on the AMC is described in detail. Results from the study of the EGaIn channel is also presented.

Chapter 4 deals with a polarization conversion antenna. The truncated patch antenna requires designing both the antenna and its feed, which are explained using accompanying figures and graphs. Simulation results of the antenna switching between linear and circulation polarization with relevant explanation is presented.

Chapter 5 concludes the thesis by listing out the contributions and the different designs that demonstrate reconfigurability using the metallic fluid EGaIn. The fabrication process is summarised and is deemed to be a future step for this project. Other future designs that can be studied and implemented using this technology are also touched on for the readers

.

CHAPTER 2: BACKGROUND & LITERATURE REVIEW

2.1 Background of EGaIn

Conventional methods of reconfiguring antennas' operational characteristics have become a very flushed out field, with numerous designs achieving multiple kinds of reconfiguration. Techniques such as integration of varactor or p-i-n diodes, use of magnetic materials, employment of MEMS, etc., have all been investigated excessively. Building a comparison with all those technologies would be laborious and stray the reader from the central point of this thesis. Therefore, the focus of this chapter is kept around the RF designs that employ microfluidics or LM channels to achieve the targeted reconfigurability. Microfluidics and LM are used interchangeably for this technique. Microfluidics/LMs offer a variety of ideas with the ability to leverage some new and unique aspects. In almost all the designs found in the literature, the liquid chosen for antenna applications have a few common characteristics. The metals posses a high electrical conductivity (above 10^6 S/m) and are formed from the alloys of Gallium or Mercury. This greatly narrows the candidate for this thesis. The most commonly used among them is eutectic 75% Gallium 25% Indium (EGaIn). It has a conductivity of 3.4×10^6 S/m, and its fluid nature gives the designer the ability to use this high conductivity in innovative ways [17]. It is noteworthy to mention it here that the conductivity of this metal is one-ten folds less than what is expected from conventional metals like copper, silver etc. However, the fact that these metals exist in the liquid form is bound to change some of their characteristics. Nevertheless, the value expressed here is decent enough for the applications that are envisioned for this work.

Typically, antenna designers control the flow of EGaIn by designing channels around the radiating element within the substrate. The shape, position, and location of the channels can be used to influence currents on the radiating element and achieve the desired level and type of reconfiguration [18]. The literature, that is to be covered herewith, shows channels integrated in different ways, such as, within the substrate, part of a metasurface, integrated within the antenna, etc. Using these channels designers have used LMs to achieve frequency and bandwidth modulation, pattern diversity, and polarization reconfigurability. All these outcomes have opened new venues for the designers to investigate the antennas that rely on these microfluidic channels.

2.2 Literature Review of Reconfigurable Designs Using EGaIn

One of the earliest publications that showcase the use of EGaIn in antenna design is presented IEEE Antennas and Wireless Propagation Letters [19]. The designers integrated small channels called capillary tubes within the antenna substrate between the printed metal (the conventional metal layer), Fig. 2.1. The LM would flow through these channels and act as the radiating element to form a cross-dipole structure, shown in the bottom right of Fig. 2.1 (a). The length of the dipoles' arms can be controlled using a bias voltage applied at the ends of the capillary tubes, circled in red in the figure. This method of LM control is referred to as electrochemically controlled capillarity (ECC) and gives the scope for continuous tuning. By varying the bias voltages for two dipoles separately, frequency tuning for two separate bands can be achieved. The impedance performance of the proposed the design is shown in Fig. 2.1 (b) to (d). The bias voltages correspond to a specific dipole length and if both the lengths are close, a crossed dipole can produce CP due to the normal current configuration in the two arms. The authors accomplished

this, giving their system continuous frequency tuning from 0.8 to 3 GHz and circular polarization conversion from 0.89 to 1.63 GHz.

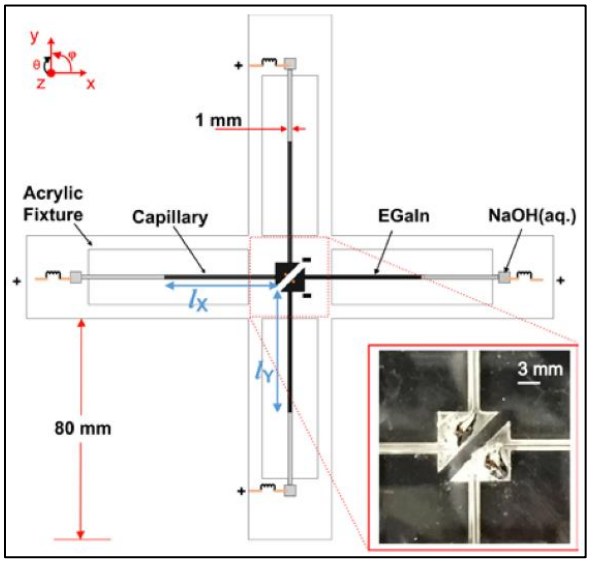

(a)

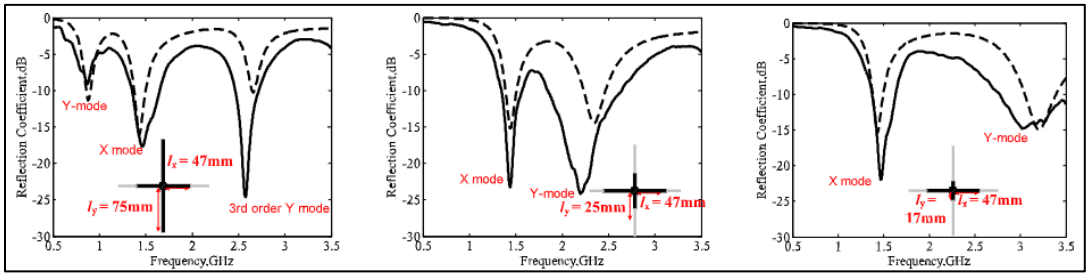

(b) (c) (d)

Fig. 2.1 Cross Dipole Antenna (a) Design and Prototype (b)(c)(d) Tuning from Dipole Length [19]

The shape of the antenna is another important consideration for designing such channels. This is evident from the design published in [20], Fig. 2.2 (a). A conical antenna is used with vertical poles to serve as the LM channels achieving pattern reconfiguration, seen from the graphs of Fig. 2.2 (b). The designers are able to control the height of LM, thus creating poles for antenna radiation. These poles result in changing the beamwidth of the

principal pattern and also rotating the radiation along the azimuthal plane. In total, the system provides 21 different states, some of which are shown in Fig. 2.2 (b). Interestingly the frequency of the antenna remained stable at around the center frequency of 2 GHz. Thus, maintaining impedance performance for various states.

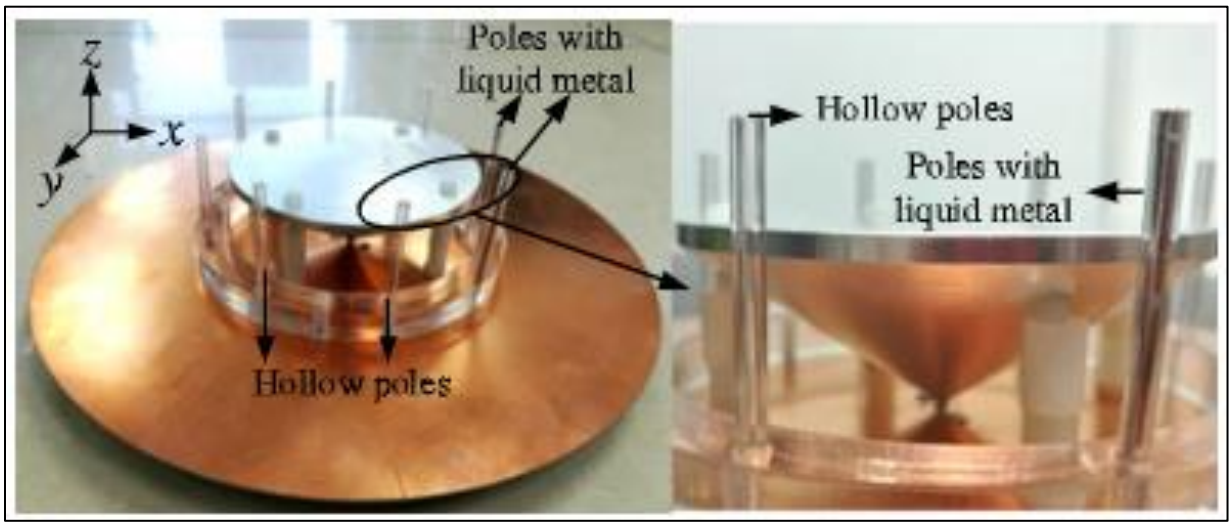

(a)

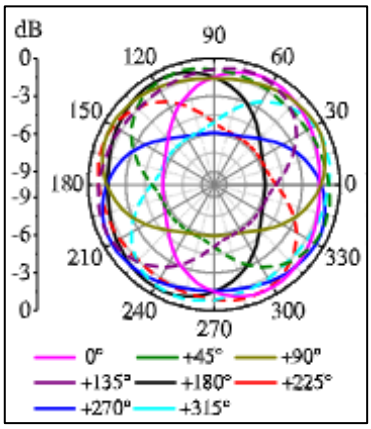

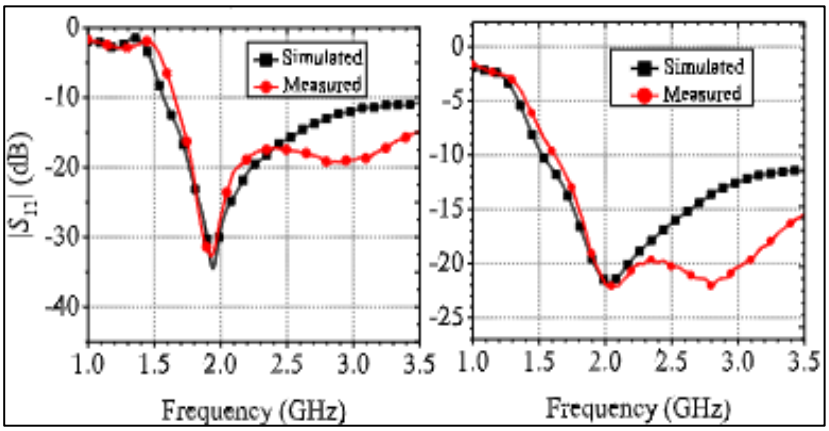

(b) (c)

Fig. 2.2 Conical Antenna (a) Design and Channel (b) Radiation States

(c) Different EGaIn Pole Height [20]

Another interesting variation of microfluidics-based design is presented in [21]. The authors of have designed cavities across the width of the antenna to compliment a truncated patch antenna's structure, shown in Fig. 2.3 (a). The idea is to provide the system with radiation polarization agility when the channels are filled with the LM. Instead of using the classical truncated patch on the corners of a square patch, Ecoflex cavities are used in the design. A photograph of the fabricated antenna prototype in a circular polarization state, with EGaIn filled in diagonally opposite cavities is shown in Fig. 2.3 (b). The aperture fed patch is designed to generate LP radiation, as seen in Fig. 2.3 (f).

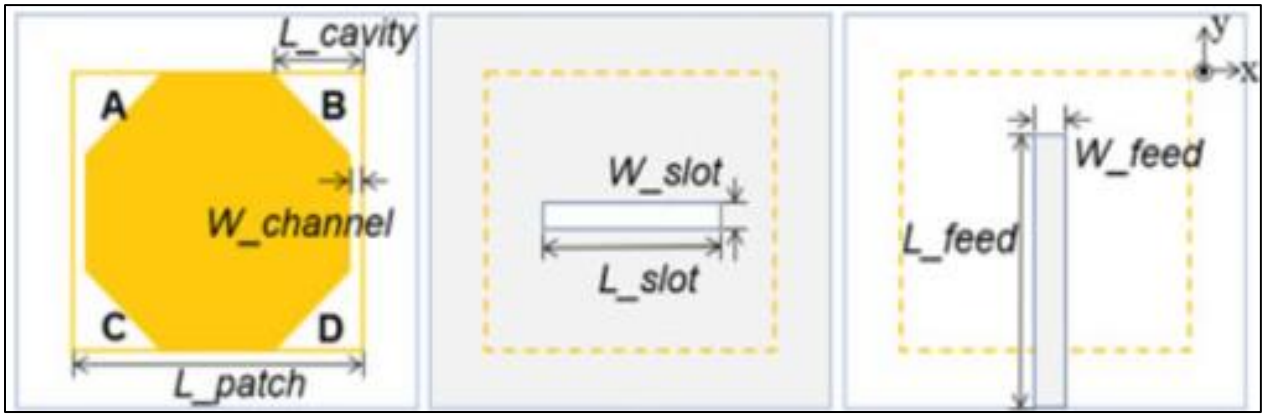

(a)

(b)

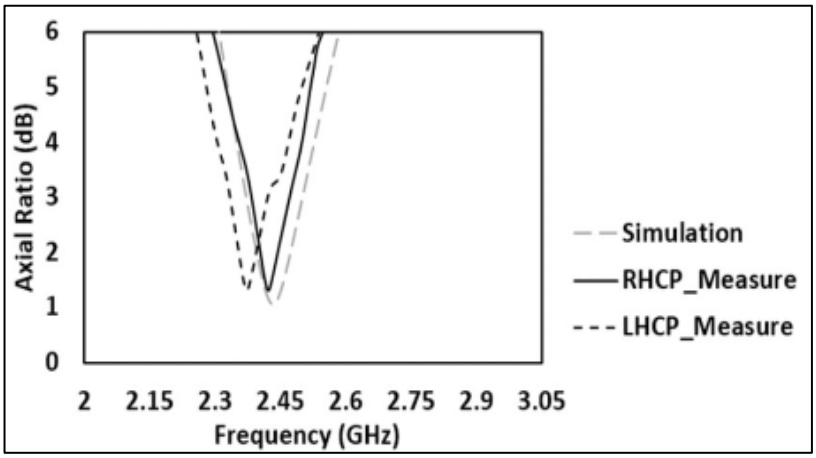

(c)

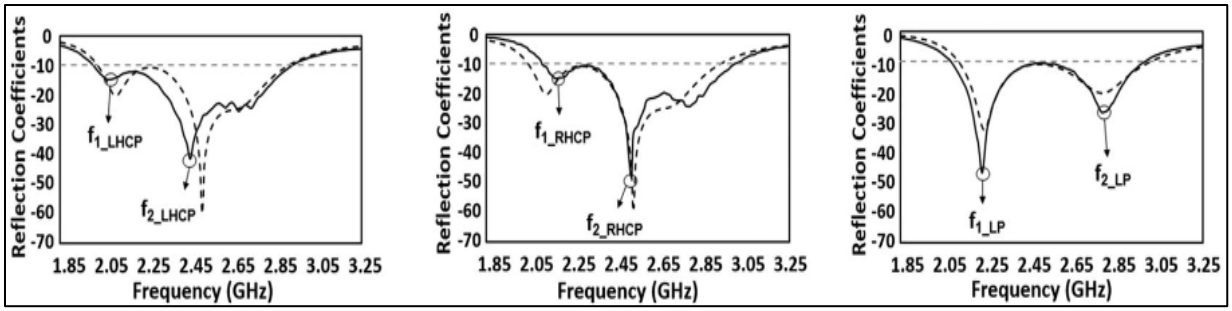

(d) (e) (f)

Fig. 2.3 Reconfigurable Patch Antenna (a) Design Stackup (b) Fabricated Prototype

(c) Axial Ratio S_{11} Responses (d) LHCP (e) RHCP (f) LP States [21]

Next, the authors selectively fill the cavities to generate different types of circular polarizations, shown in Fig. 2.3 (d) and (e). The antenna maintains stable bandwidth performance which is essential in such a reconfigurable design. However, the authors did not discuss the axial ratio (AR) vs. frequency plot which would be useful for evaluation of such a design. This in no-way reduces the significance of the proposed antenna structure.

In a subsequent patch antenna radiator of [22], the focus is to alter the radiation modes of the antenna (shown in Fig. 2.4 (a)). The authors of intentionally etched slots in the metal surface of the antenna to disturb or in other words to excite the desired mode of radiation. The target is to convert a TM10 to a TM30 mode, as seen in Fig. 2.4 (c). Using channels printed inside a polyester lined acrylic layer the modes are reintroduced slowly by letting EGaIn flow through the channels. The complete antenna system is design on a Rogers 5880 board which is known for efficient antenna designs. Fig. 2.4 (b) shows the different working frequencies the antenna can achieve by varying the portion of slots that the EGaIn is covering. The authors can achieve dual-band operation by separately controlling the channels on the top or bottom of the patch.

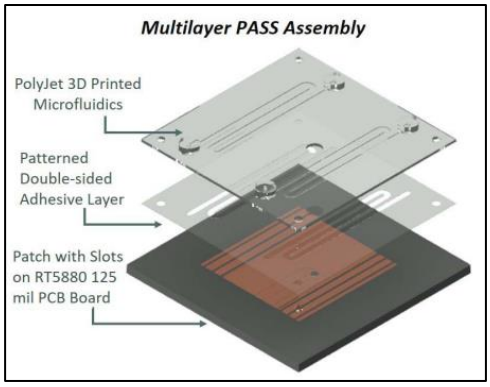

(a)

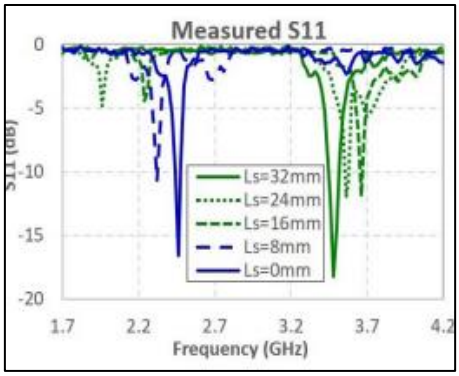

(b)

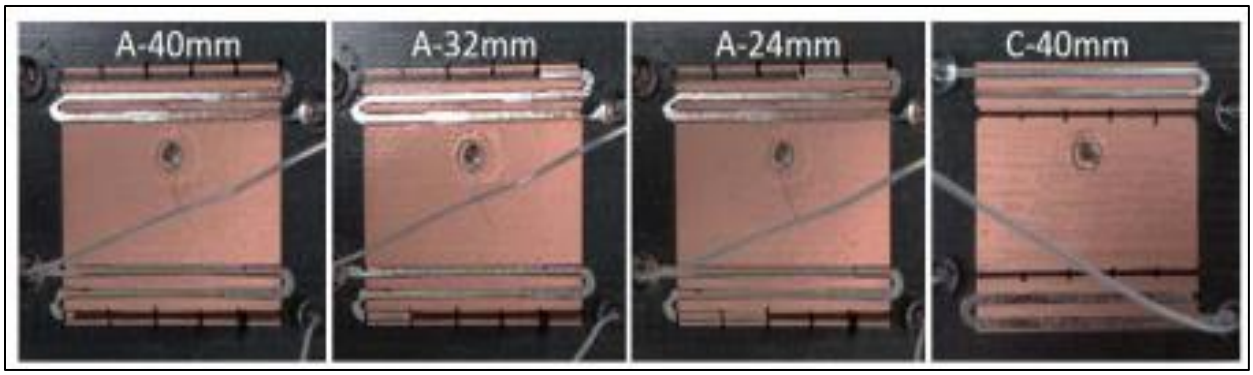

(c)

Fig. 2.4 Square Slotted Patch (a) Antenna Design (b) Substrate Stackup (c) S11 Results [22]

Channels can also be made in multiple layers, as seen in [23], where the authors used two separate layers to induce left-hand (LHCP) and right-hand (RHCP) circular polarization over a square ring patch antenna. The channels are inside two polydimethylsiloxane (PDMS) layers and are positioned at an angle of 45˚ to the fields on the patch, shown in Fig. 2.5 (a). Each layer of PDMS further contains 5 different channels, labelled L_{s1}, $L_{s2,}$ etc., which can be filled separately to choose a different operating state. Therefore, by choosing between two polarization layers and then choosing among five frequency-shifting microchannels, the authors describe 6 different states between 2.4 and

2.9 GHz, shown in Fig 2.5 (b) & (c). The authors have also elaborated on the challenges that are encountered in prototype fabrication and the consequent measurement of their

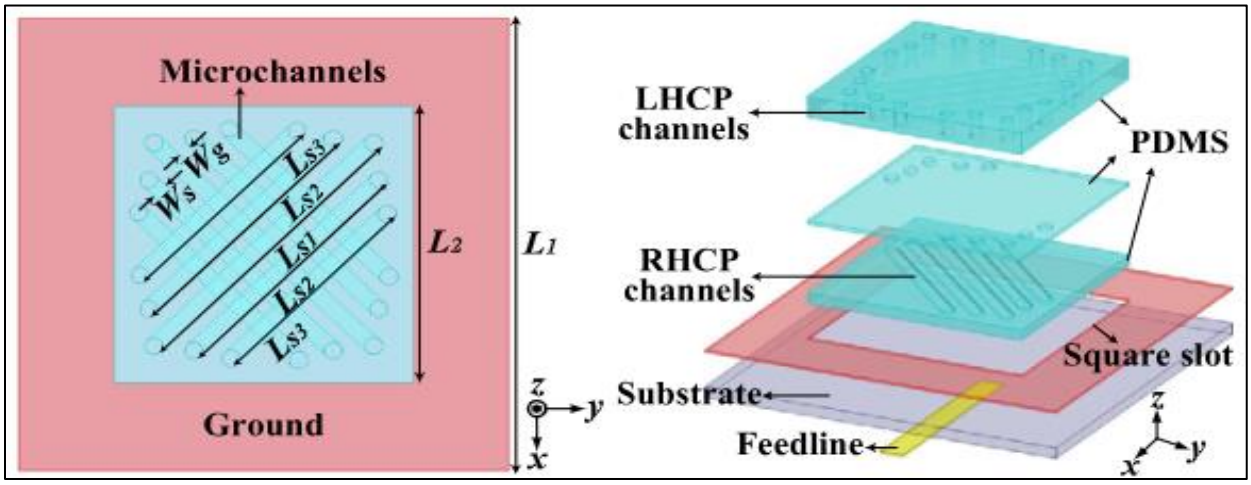

(a)

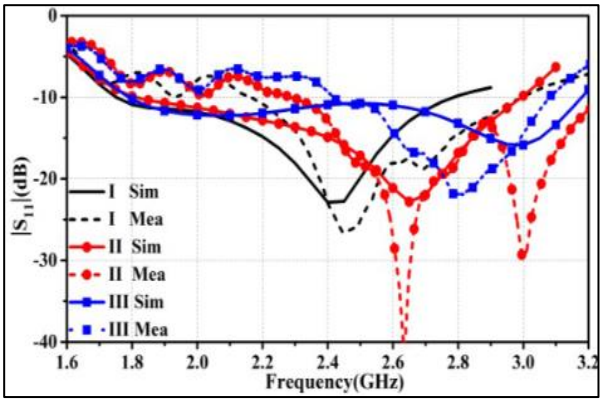

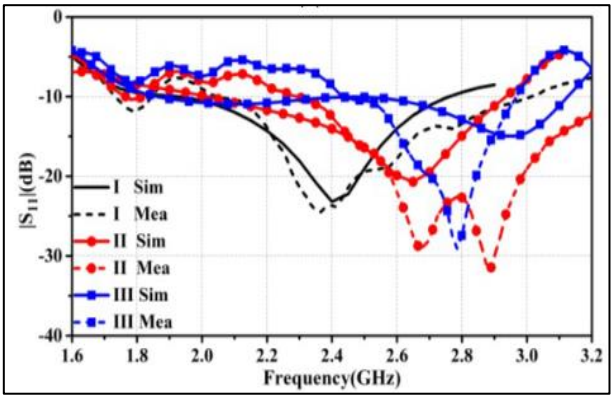

(b) (c)

Fig. 2.5 Square Ring Patch (a) Substrate Stackup (b) S11 Response with LHCP Channels

(c) S11 Response with RHCP Channels [23]

proposed structure. This type of analysis and discussion is especially useful for such designs as it can provide a sound guideline to the aspiring designers by filling the void of shallow literature.

The EGaIn channels can also be used as the parasitic elements of a radiator such as Yagi-Uda antenna, Fig. 2.6 [24]. A conventional Yagi-Uda antenna has an active dipole that is primarily responsible for antenna radiation. Furthermore, it consists of two or more passive dipoles that are used to enhance the gain and shape the directive antenna beam. One passive dipole acts a reflector, and the other dipole acts as a director, and together they enhance the gain of the antenna system. More than one director can be used based

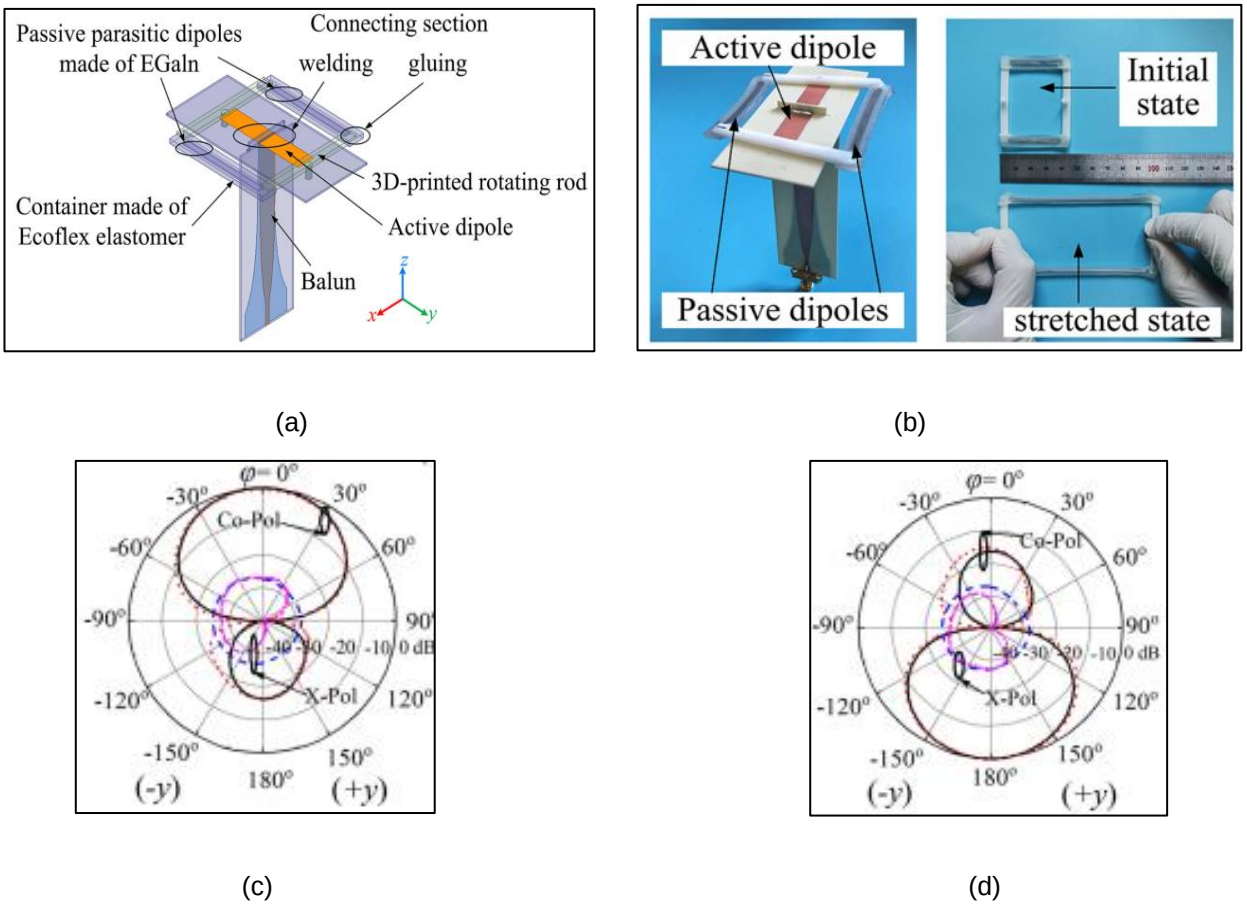

Fig. 2.6 Modified Yagi-Uda Antenna (a) Design (b) Channel States

(c) +5° Balun Rotation (d) -5° Balun Rotation [24]

on the size constraints and gain requirements of the antenna. In [24], the authors accomplish this gain enhancement by exploiting the use EGaIn microfluidic channels that

can change the length of passive, shown in Fig. 2.6 (b). The active dipole is fed by a balun structure that can rotate 5˚ in either direction, allowing each EGaIn channel to function as a director or reflector. By altering the balun direction, radiation pattern diversity can be achieved, as seen in Fig. 2.6 (c) & (d).

The channels can also be placed directly on top of the slots to have a better control over the amount of EGaIn present on the radiating structure, as shown in Fig. 2.7 (a) [25]. By venturing the use of polytetrafluoroethylene (PTFE) tubing, EGaIn liquid metal is injected into 3D printed channels that are strategically placed around an E-shaped patch antenna, shown in Fig. 2.7 (b). Using VeroClear acrylic material, the 3D printed channel is placed with 0.5 mm gap between the LM and the antenna copper. The antenna produces LHCP radiation which can be gradually altered to a rotated LP radiation by varying the slot lengths. This is accomplished in the design with the movement of EGaIn over two separate sets of slots, producing 1 state with LHCP and 5 states with LP (angled at 10˚ to 45˚), shown in Fig 2.7 (c) & (d).

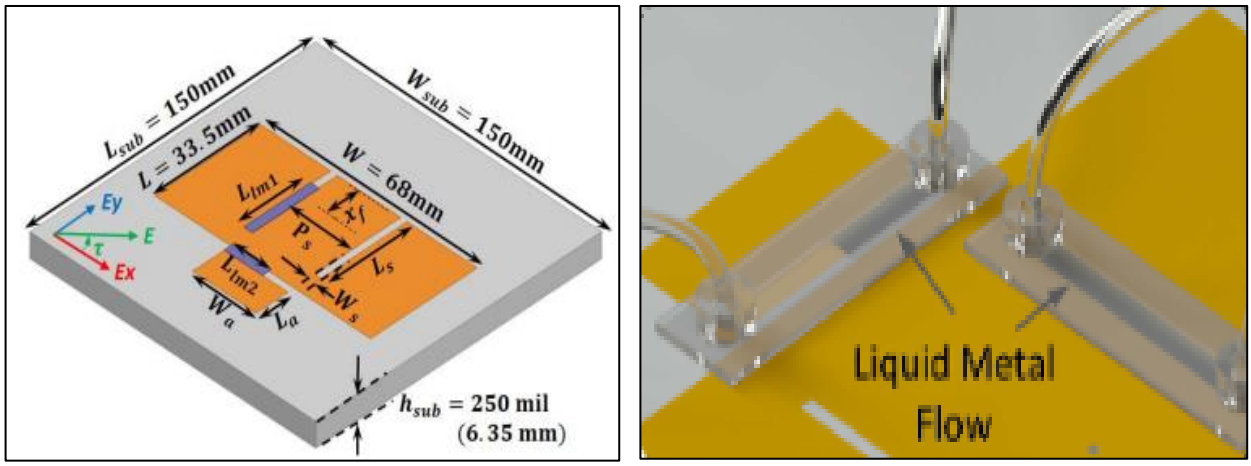

(a) (b)

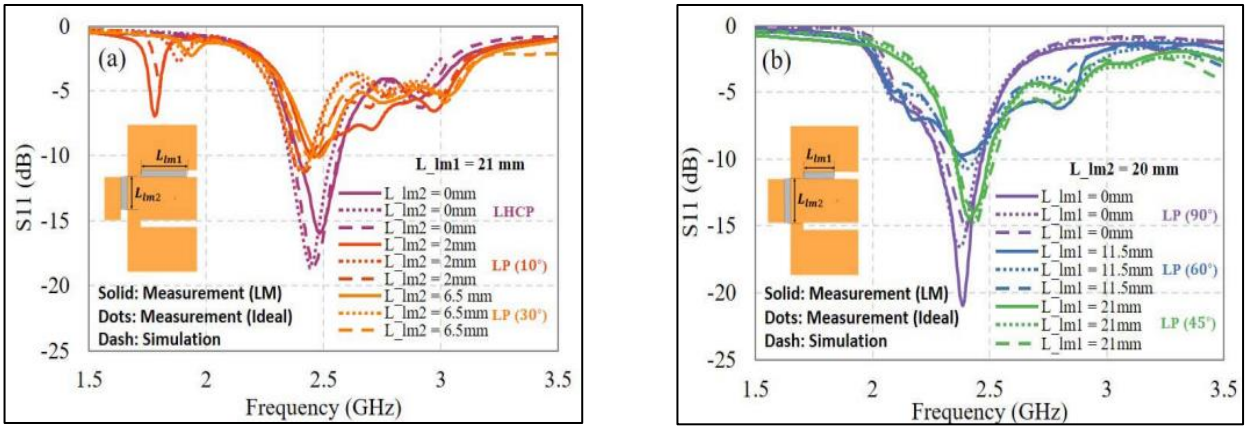

(c) (d)

Fig. 2.7 Slotted Patch Antenna (a) Design (b) PTFE Tubing and Channel Placement

(c) LHCP & (d) LP States [25]

As a last example of this literature review, an antenna specifically targeted for a medical application is included in this discussion [26]. A PDMS layer with branches of EGaIn channels is placed above a slot antenna formed from a conductive mesh, Fig. 2.8 (b). Along with the antenna, the PDMS layer and EGaIn channels are designed to be flexible, that leverages its use in the intended application. Analysis of the surface current on the branches shows how the antenna can produce three states in the Industrial Scientific Medical (ISM) band, seen from the graphs in Fig. 2.8 (a). The LM channels can induce a circular current to have LHCP and RHCP, one example shown in Fig. 2.8 (c), while the vacuum state produces LP radiation. The designers also test the design for near human body applications, shown in Fig. 2.8 (d). The specific absorption rate (SAR) of their design is found to be approximately 0.4 W/kg, which is below the standard of 2 W/Kg, effectively demonstrating the non-toxic nature of EGaIn. However, it should be mentioned that the results thus presented are of initial nature and would require more elaborated testing to be employed in the final application.

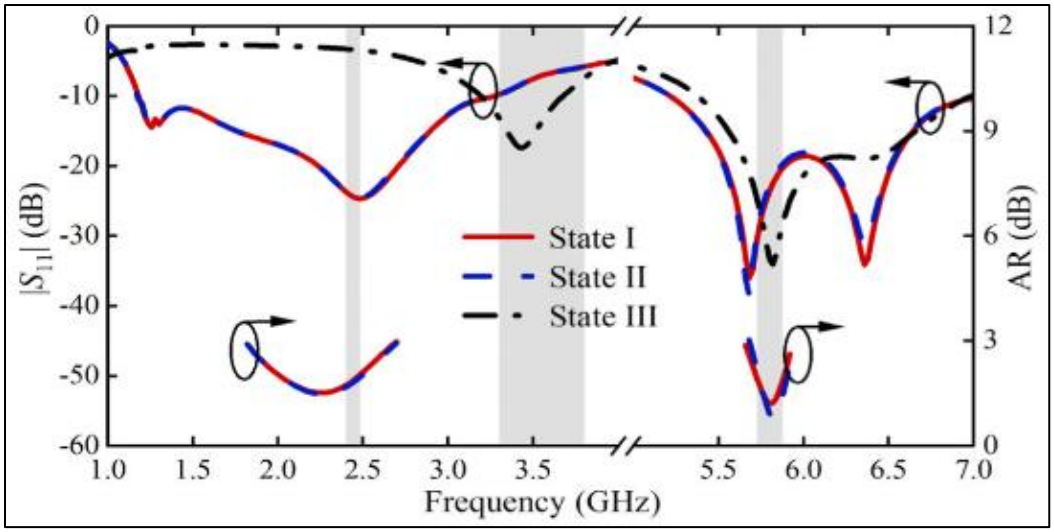

(a)

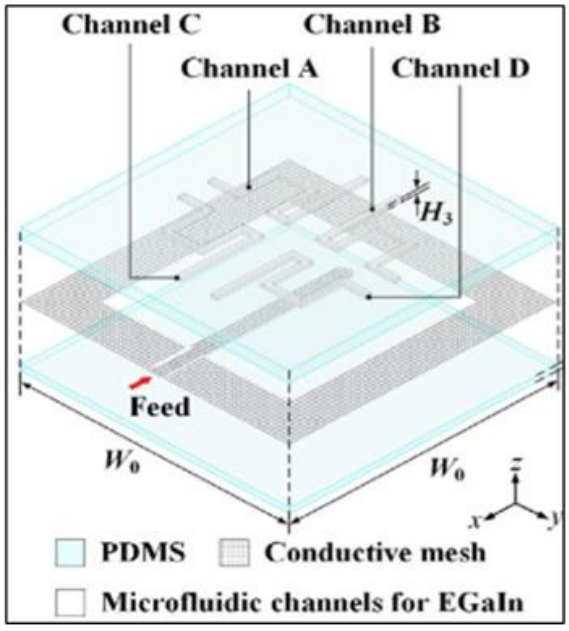

(b)

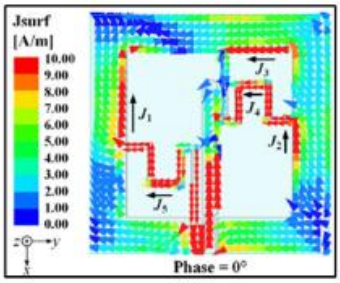

(c)

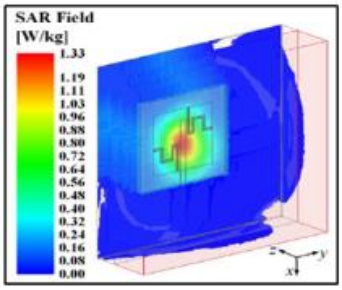

(d)

Fig. 2.8 (a) Ring Antenna with PDMS Layer (b) Surface Current with EGaIn (c) SAR Results [26]

A summary of the literature that revolves around the topic of microfluidic or LM channels is provided in Table 2-1. The readers can quickly deduce that most of these publications are in the last 5-7 years time frame that emphasizes the novelty of this technique.

Table 2-1 Comparison of EGaIn Based Antenna Designs

Reference (year of publication)	Operation Frequency (GHz)	Type of Reconfiguration	Gain (dBi)	Bandwidth (GHz)	EGaIn Channel
[20] **(2018)**	1.7-2.7	Radiation pattern	6.7	1	PMMA reflectors
[24] **(2021)**	2.4-2.48		6	0.04	Elastomer reflectors
[21] **(2018)**	2.45	Polarization	7	0.73	Ecoflex cavity
[25] **(2020)**	2.3-2.6		7	0.3	PTFE, acrylic
[27] **(2022)**	8-12		--	8	Acrylic metasurface
[26] **(2024)**	2.45, 3.5, 5.8		-1.7, -5, 2	2	PDMS metasurface
[22] **(2019)**	2.3-3.2	Frequency	7	0.4	3D printed metasurface
[28] **(2024)**	4-12		1	4	Resin
[19] **(2017)**	0.8-3	Frequency, Polarization	0.3-1.7	2.3	Capillary tubes
[23] **(2020)**	2.4-2.9		4	0.3	2 PDMS metasurfaces
[29] **(2021)**	8-32	Phase	--	24	Silicone metasurface

2.3 Conclusion

The different designs reviewed show a variety of reconfiguration techniques along with associated manufacturing processes. The channels have been constructed using a

variety of materials namely, acrylic, polymethyl methacrylate (PMMA), silicone, PDMS, etc. On the other hand, conventional methods of reconfiguration have been extensively researched with reliable design procedures and methodology. However, the review has also shown that the field of LMs is only beginning to mature, with a lot of different methods of reconfiguration still left to explore. With most novel methods of antenna reconfiguration, impedance switching is often the first and easiest that designers can achieve. The review has also reveled several designs achieving polarization agility. Most systems have different states with vacuum and EGaIn channels and this state switching behaviour is well suited for polarization conversion. Therefore, the following chapters contain two methods for achieving reconfiguration using LMs, namely impedance switching and polarization conversion.

CHAPTER 3: FREQUENCY SWITCHABLE ANTENNA

Against the backdrop of the literature review presented in the last chapter, this thesis focusses on the design of microfluidic based antenna systems. For this purpose, two different designs are studied herewith. The first one being the impedance or frequency switchable antenna and the latter one is a polarization reconfigurable design. Since the two designs have distinct differences from each other and in their design procedures/analysis, it is prudent to discuss them in separate chapters starting with the first one between the two.

3.1 Overview of the Design

The impedance controllable/switchable design relies on a patch antenna that is backed by a reconfigurable AMC structure as shown in Fig. 3.1 (a). The stack up of the substrate used for this design is elaborated in the next figure, i.e., Fig. 3.1 (b). It consists of two layers of Rogers 5880 substrate (ε=2.2) that sandwich an acrylic layer (ε=3.4) between them. The acrylic layer can be regarded as the functional layer in this design as it contains the channel for the LM. The metallic layers on the substrate are to be realized using the 5880 PCB boards. It can be observed that there are 3 metal layers in total, the antenna on the top, the AMC layer in the middle and the ground plane at the bottom. The shape of the antenna and the AMC are illustrated with the help of Fig. 3.1 (a). It is well-known that an AMC backed antenna provides improved gain response as compared to the design without one. So, this is expected in this case. The structure of AMC used herewith is inspired from an existing article [30]. The goal for this design is to modify the AMC structure by employing the microfluidic channel in acrylic. The red colored spiral-shaped channel is used to add this functionality to the design. The frequency of operation of a

patch antenna is dependent on the electric fields created inside the substrate. Thus, by disturbing the field structure/pattern, one can control the center frequency of the antenna. This is achieved in this design, shown in Fig. 3.1 (a), by using LM channels underneath the antenna, causing the antenna to function normally with vacuum channels (no metal) and switch to another frequency with EGaIn (metal used in this case) channels.

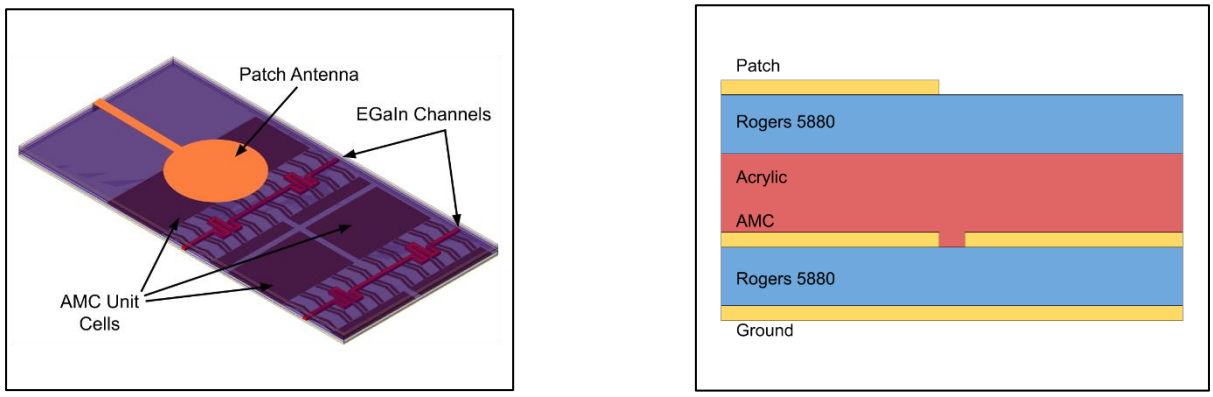

(a) (b)

Fig. 3.1 Impedance Switchable Antenna (a) Design (b) Substrate Stackup

The LM channels are placed at the bottom of this acrylic substrate and changing it from vacuum to EGaIn achieves reconfigurability. The design is simulated in Ansys' High Frequency Structure Simulation (HFSS) to obtain the results shown in the sections below. The design process of the antenna, AMC, channels, integration of different components, simulation setup and results are discussed in the sections to follow.

3.2 Circular Patch Antenna

The literature review revealed multiple types of antennas being used in reconfigurable designs. However, with many designs, the method of reconfiguration is specific to the geometry of the antenna being used. A generic structure that can achieve the same

reconfiguration with any type of patch antenna is rare. Therefore, the antenna selected for this design is a monopole circular patch antenna with a uniform radiation pattern, shown in Fig. 3.2 (a). This type of a design simplifies the fabrication of the antenna structure where the channels in the acrylic are bound to provide some challenges. The antenna is designed on the same substrate stack shown in Fig. 3.1 (b) and is targeted for the ISM frequency band (~2.5 GHz).

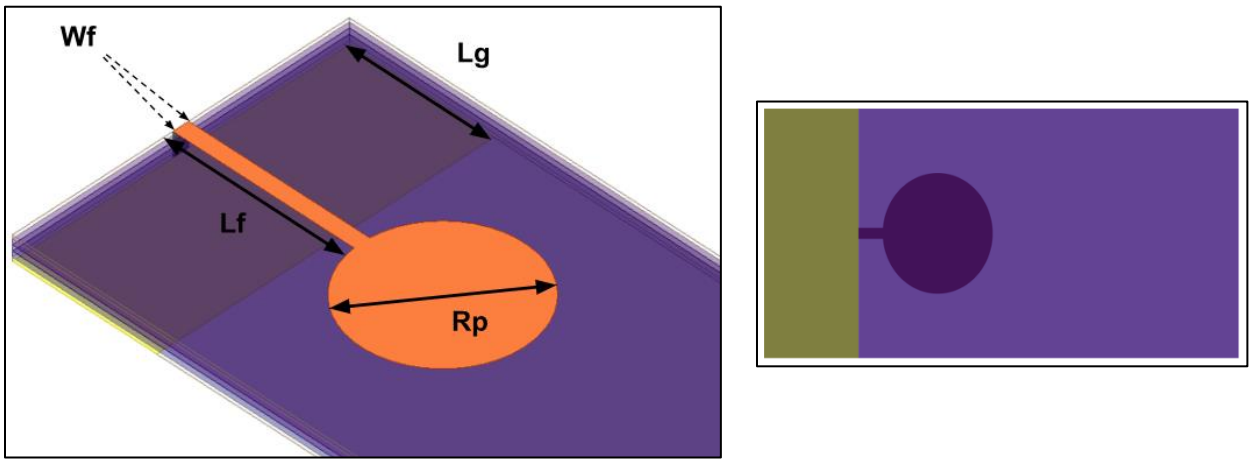

(a) (b)

Fig. 3.2 Monopole Patch Antenna (a) Dimensions (b) Bottom View

For a monopole antenna, the two important parameters that control the frequency of operation are the dimension of the antenna and the size of the ground plane. Between these, the ground plane actually plays a more dominant role. Thus, the pronounced focus of the design analysis is centered around the ground plane dimensions. Parametric analysis of other features such as patch radius, feed length, feed width, etc. is also performed in this work. However, much of the optimization is possible exclusively through the ground plane length. To demonstrate this, a parametric analysis of the ground length is shown in Fig. 3.3, where the length of the ground plane is varied from 24 mm to 41 mm.

The center frequency of the antenna and its bandwidth change with this changing length. This is expected because the ground plane of a monopole antenna basically signifies the input impedance seen by the excitation port. Thus, the change in the impedance performance of the antenna. The results obtained here conclude that a ground plane length of *Lg=24 mm* provides the most optimum results for the antenna.

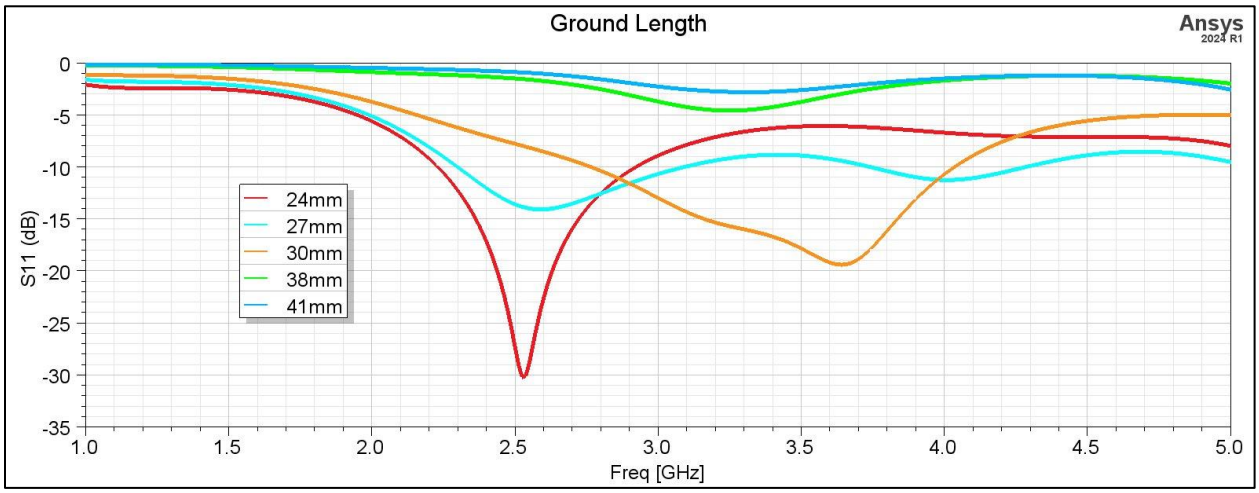

Fig. 3.3 Parametric Analysis of L_g

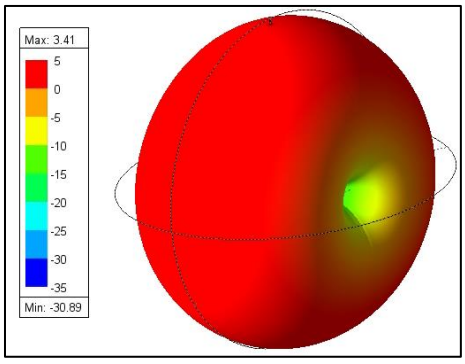

Fig. 3.4 Gain and Radiation Pattern at 2.5 GHz

The next logical step is to observe the radiated fields from the monopole to ascertain that the antenna is indeed working at the targeted frequency. From Fig. 3.4, it can be deduced that the antenna radiates with a donut-shaped radiation also referred to as omni-

directional pattern. This is in line with the expectations from a monopole antenna. A maximum gain of 3.47 dBi is achieved at 2.5 GHz. The higher gain than a conventional wire monopole is expected as this is a patch-based monopole radiator. With the integration of the AMC, this gain is expected to increase for both the antenna's design frequency (2.5 GHz) and the switching frequency (1.65 GHz). Likewise, the other parameters of the antenna are optimized in a sequence as explained for the case of ground plane length. To avoid repetition, the author would just like to provide a table that summarizes the dimensions of the stand-alone antenna.

Table 3-1 Dimensions of Optimized Circular Patch Antenna

Variable	**Dimensions** (mm)
R_p	27
L_f	30
L_g	24
W_f	2.6

3.3 Artificial Magnetic Conductor Design

An artificial magnetic conductor is a high impedance surface that can reflect radiation belonging to a specific frequency. When used in an antenna system, the reflected radiation combines with the incident wave resulting in gain enhancement of the antenna. There are quite a few publications that explain the operation and a variety of designs that rely on AMC structures [4], [30], [31], [32]. A simple AMC design that has been dominantly used in publications is based on a mushroom-like structure, shown in Fig. 3.5 (a), in the place of a conventional copper ground plate. The mushroom structure offers an inductor-capacitor circuit to the incoming radiation, performing a filtering function. A zoomed version of the design shows some of the inductances and capacitances of the unit cells. The structure consists of repetitive unit cells formed by copper sheets mounted on top of

vertical metal vias, shown in Fig 3.5 (b). The spacing and dimensions of the unit cell determine the resonant frequency of the combined AMC structure. By changing the size of the square unit cell, the inductance *'L'* experienced by an impinging incident wave can be changed. Similarly, by placing the unit cells at different distances from each other, the capacitances *'C'* generated between them can also be changed/controlled. The combined inductances and capacitances generated from the entire AMC structure forms a resonant circuit with a resonance frequency 'ω_0' that can be obtained from the following equation,

$$\omega_0 = \frac{1}{\sqrt{LC}}$$

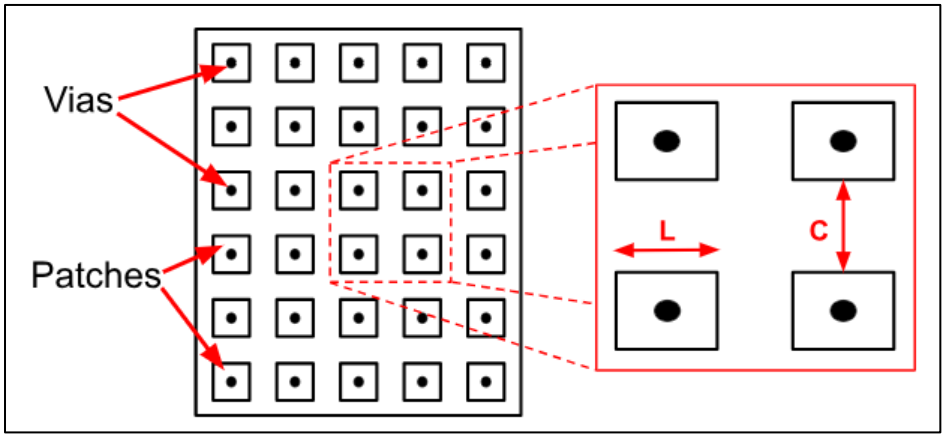

(a)

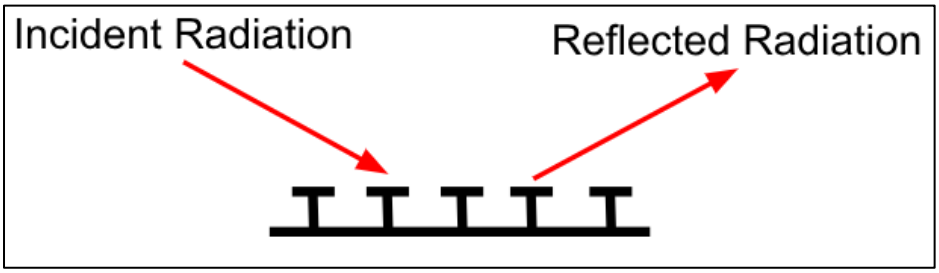

(b)

Fig. 3.5 Mushroom AMC Structure (a) Top View (b) Side View

Radiation with this resonant frequency is reflected towards the antenna and is responsible for the gain enhancement characteristic of an AMC. The reflected radiation encounters the antenna's forward radiation and the phase difference between them determines the type of recombination experienced here, figuratively explained with the assistance of Fig. 3.6 (a). The phase response of the reflection coefficient of an AMC structure is shown in Fig. 3.6 (b). With a phase difference of 0°, the incident and reflected radiation can combine constructively to maximise the gain of the antenna in the incident direction. In practise a phase difference of ±45° provides noticeable gain enhancement and is generally employed in the designs found in literature [4], [30], [31], [32]. By moving the AMC towards or away from the antenna, the distance travelled by the reflected wave can be changed, giving a designer the ability to control the phase difference and maximise the resultant gain. However, this distance is not a flexible variable as it depends on the thickness of the substrate.

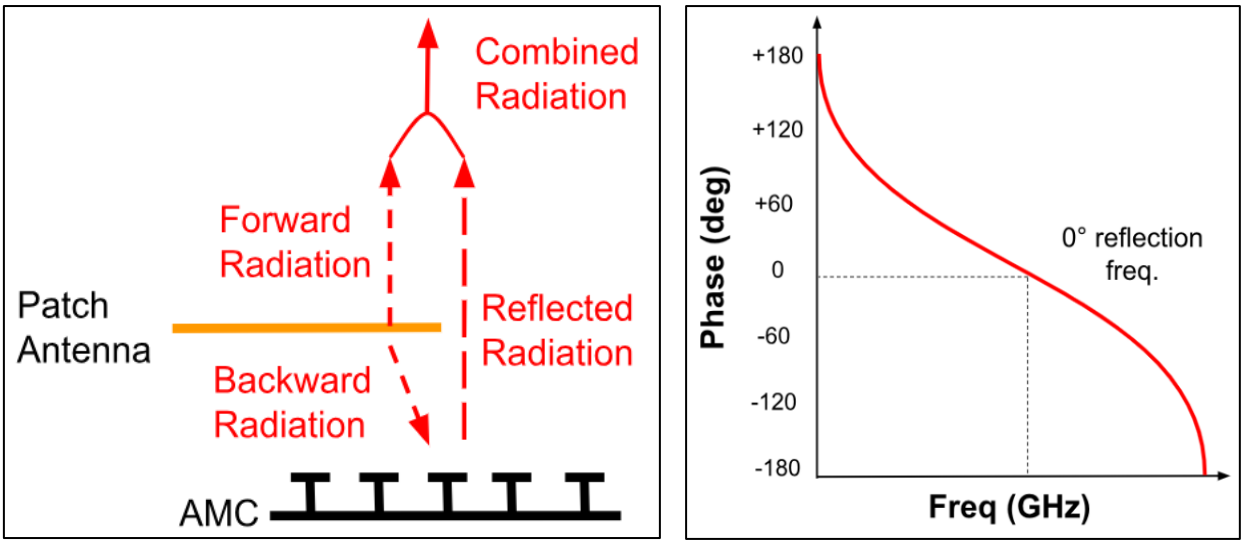

(a) (b)

Fig. 3.6 Functioning of AMC (a) Cross Sectional View of Antenna & AMC (b) Phase Response of AMC

Therefore, when designing an AMC structure, one needs to carefully optimize the gap between the AMC layer and the ground plane that matches with the substrate thicknesses that are reasonable implementable. The preliminary AMC unit cell, used for this thesis, is shown in Fig. 3.7. It is simulated in Ansys HFSS environment with a modal network that allows for the setup of a floquet port. A floquet port emits a plane wave as if it is radiated from an antenna in the far field. The wave impinges directly onto the surface of the AMC cell as can be seen from Fig. 3.8 (a). The AMC unit cell is inspired from the design in [30] due to its frequency of operation and the presence of strips between the two large patches for channel interaction. As explained previously, the periodic repetition of the AMC unit cell contributes to its functioning, and this is achieved on HFSS through a master-slave boundary condition.

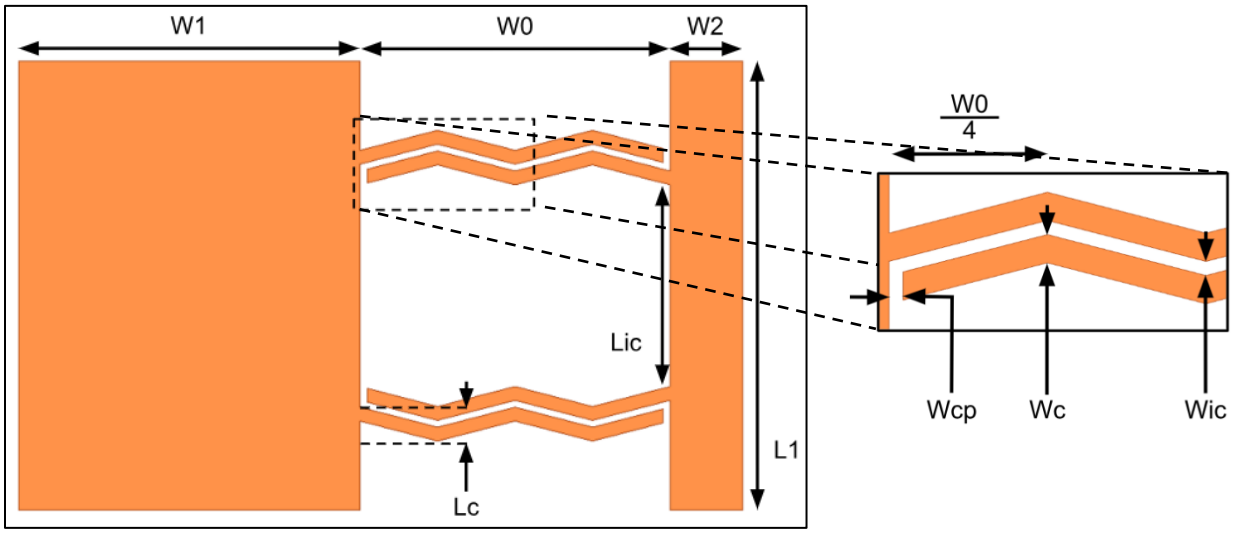

(a) (b)

Fig. 3.7 (a) Preliminary AMC Unit Cell Dimensions (b) Strip Dimensions

Using these boundary conditions, one set shown in Fig 3.8 (b), the unit cell can be periodically repeated in the *X* and *Y* directions to form the larger AMC structure which can

be placed underneath the monopole antenna. Thus, the setup imitates presence of an infinite array of AMC structure on which an EM wave is incident, and the effect of this structure is analyzed with the help of the reflected wave by measuring the reflection coefficient on floquet port.

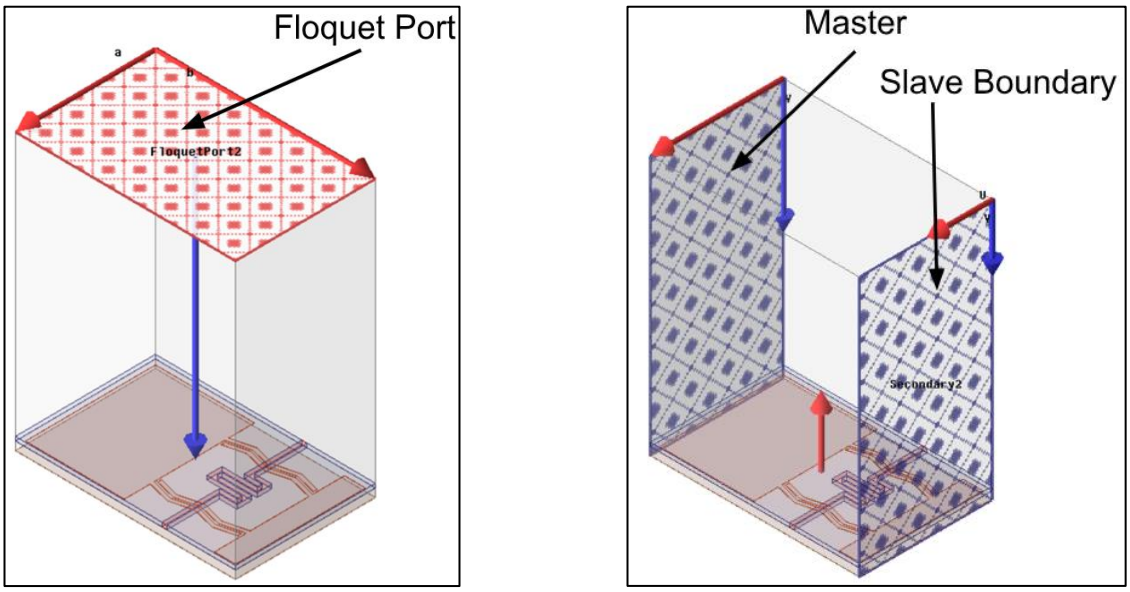

(a) (b)

Fig. 3.8 (a) Floquet Port (b) Y Axis Master Slave Boundary

The novelty introduced in this design is the fact that the AMC structure consists of two different layers. The metallic layer is emulated by modeling it on the Rogers 5880 board, while the spiral shaped channel is realized on an acrylic substrate. The PCB layers and the acrylic board are stacked up together to work as the antenna substrate. The channel is first assigned a material definition of vacuum and then consequently changed to EGaIn (σ=3.4e+06, tanδ=0.06, height=0.79mm) to simulate two states i.e., empty and EGaIn filled channel. By changing the states of the channel, it is anticipated that the antenna impedance and thus its radiation performance would change. The initial results of these

simulations depict that the antenna frequency switches from 2.11 to 1.32 GHz for these conditions of the substrates (Fig. 3.9). There are a couple of things to be highlighted about these simulations. Firstly, the initial frequency of the AMC with the vacuum channel is not at the desired frequency of 2.5 GHz (the antenna frequency). Thus, this requires some optimization to bring about a correlation between the antenna and its AMC structure.

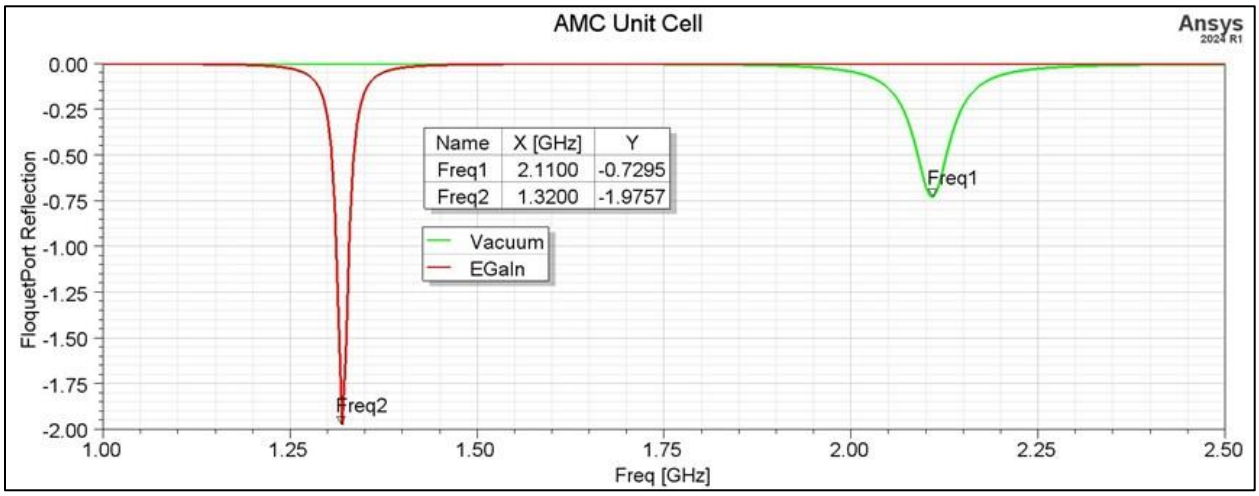

(a)

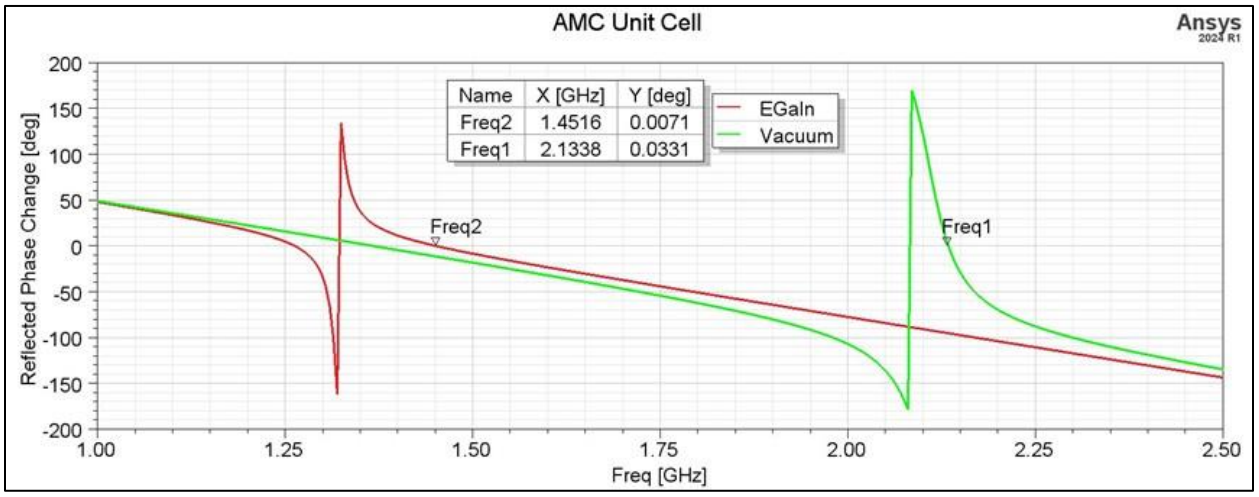

(b)

Fig. 3.9 Optimised AMC Unit Cell (a) Floquet Port Reflection (b) Phase Response

Secondly, the new resonant frequency of 1.32 GHz, although shows reflection, it does not represent the right phase of reflected wave at that frequency. Thus, both these attributes of the AMC design need to be optimized if it is to be integrated with the monopole antenna. This is taken up in the next sub-section of this chapter.

3.3.1 Parametric Analysis of AMC Unit Cell

The optimization of the AMC unit cell is necessary for this design because of a disparity between the magnitude and phase results of AMC unit cell. Following up on this discussion and comparing the markers labelled “Freq2” from Fig. 3.9 (a) and (b), the EGaIn channel state has a difference of 130 MHz between its resonance and 0° phase frequency. It is noteworthy to mention it here that for the case of the vacuum, there is a close synergy between the magnitude and phase results of reflection coefficient (labelled as Freq1). This discrepancy is arising from the AMC’s interaction with EGaIn channel and would significantly impact the gain of the antenna system. Apart from this mismatch, the preliminary AMC is also resonant at a different frequency (≈2.1 GHz) than the monopole antenna itself (2.5 GHz). The goal of the parametric analysis detailed in this section is to alleviate these issues in the design. This is done by analysing the larger dimensions of the unit cell (L1, W1, W2, etc.) and the capacitive strip in the middle, shown in Fig. 3.7 (b). The physical dimensions of the unit cell determine its resonant frequency and changing these dimensions is the most convenient method to tune the AMC’s frequency of operation. This is seen from the parametric analysis of L1 shown in Fig. 3.10 (a), with the preliminary unit cell labelled as “*Ref.=26 mm*”. As the length of the unit cell is increased, the resonance frequency is seen to be moving down. This is rationally simple to explain from the fundamentals of antenna design and is quite expected.

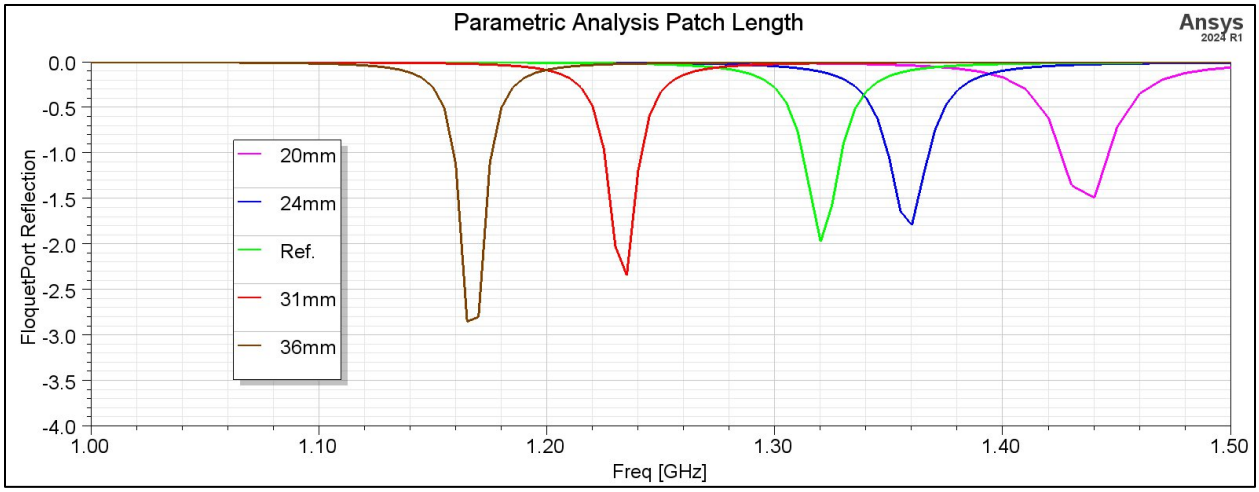

(a)

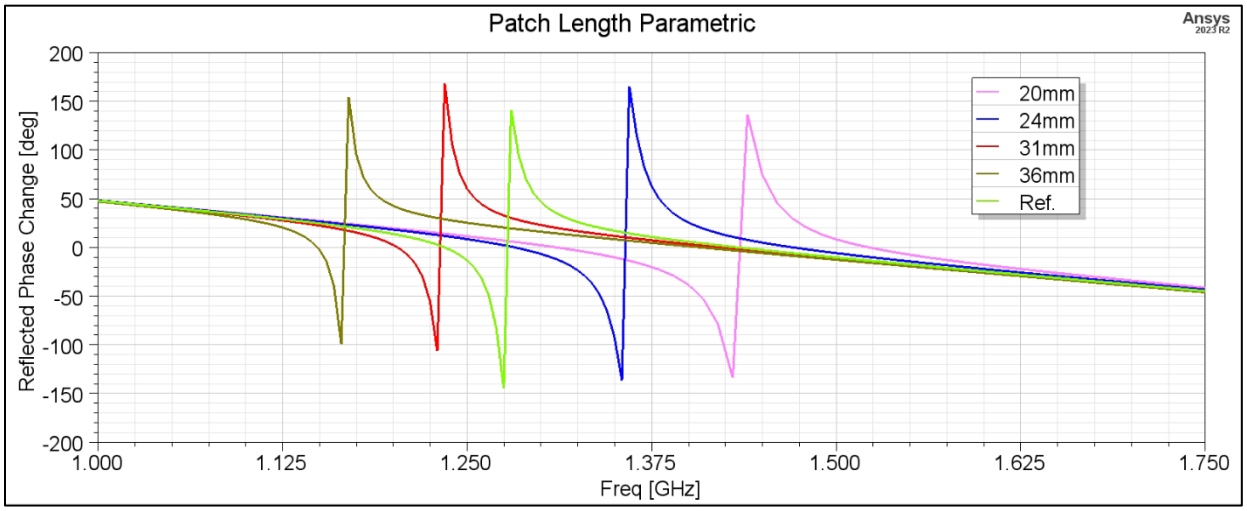

(b)

Fig. 3.10 Parametric Analysis of L_p (a) S_{11} (b) Phase Response

Thus, one can easily tune the frequency to the point of interest. While the resonance tuning achieved the correct operational frequency, the phase response is corrected using the other dimensions such as *W1* and *W2*. These show a similar pattern in results and are consistent with the fundamentals of EM wave propagation. However, it is interesting to add it here that the variables *W1* and *W2* actually control the capacitance of the AMC

unit cell and thus, play an important role in correcting the phase of reflected wave. For the sake of avoiding repetitiveness, a detailed discussion has been omitted from the section as it can be easily found in the fundamentals of antenna design and graduate students working in this field generally have a clear idea about this concept. Smaller dimensions like *OS3*, *Wc*, and *Wic* show small changes in 0° phase frequency due to small changes in capacitances.

Finally, the attention is diverted to the number of strips used in the spiral structure of the unit cell. Interestingly, the largest tuning of 0° phase is shown in Fig. 3.11 (a) and is achieved by changing the number of strips. The physical realization of two variations of the unit cell with different number of strips are shown in Fig. 3.12.

The variation in phase of the reflected wave is pictorially shown in Fig. 3.11. This change in the response of the unit cell is brought about by modifying the reactive part of the impedance due to the changing number of strips. In a nutshell, by combining these significant changes with variations in *OS3*, *Wc* and *Wic*, the 0° phase of the EGaIn state

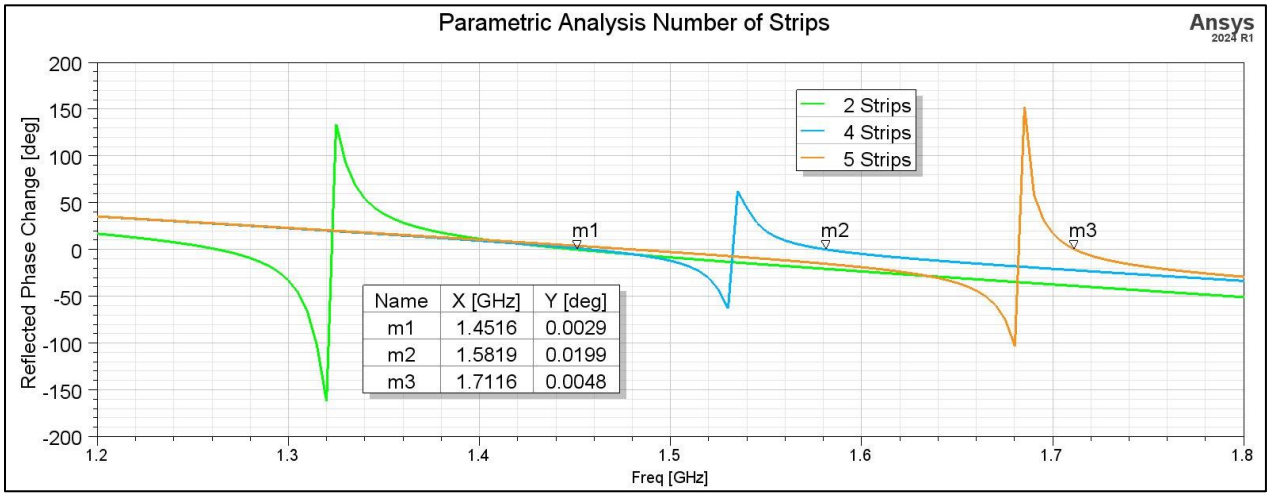

(a)

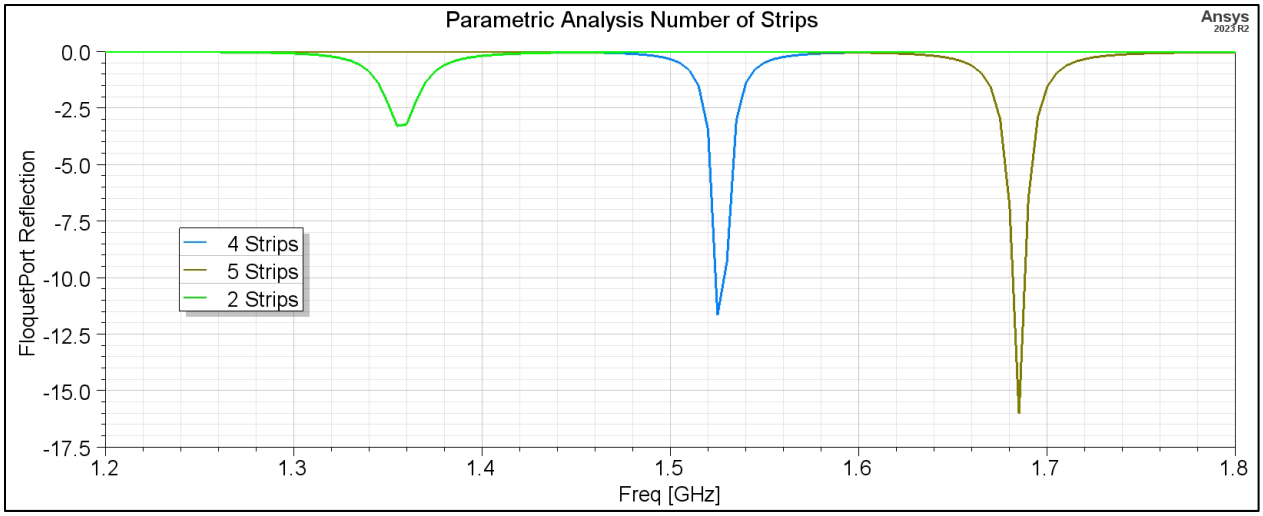

(b)

Fig. 3.11 Parametric Analysis of AMC Strips (a) Phase Response (b) S_{11}

can be controlled to reduce the mismatch mentioned at the beginning of this section. The optimised AMC unit cell is shown in Fig 3.12 (c) along with the EGaIn channel dimensions in Fig. 3.12 (d). The channel dimensions, such as *L4*, *W4*, *W5*, etc., are parametrically analysed in a similar manner to ensure that the optimised AMC works with EGaIn channel alongside the vacuum case.

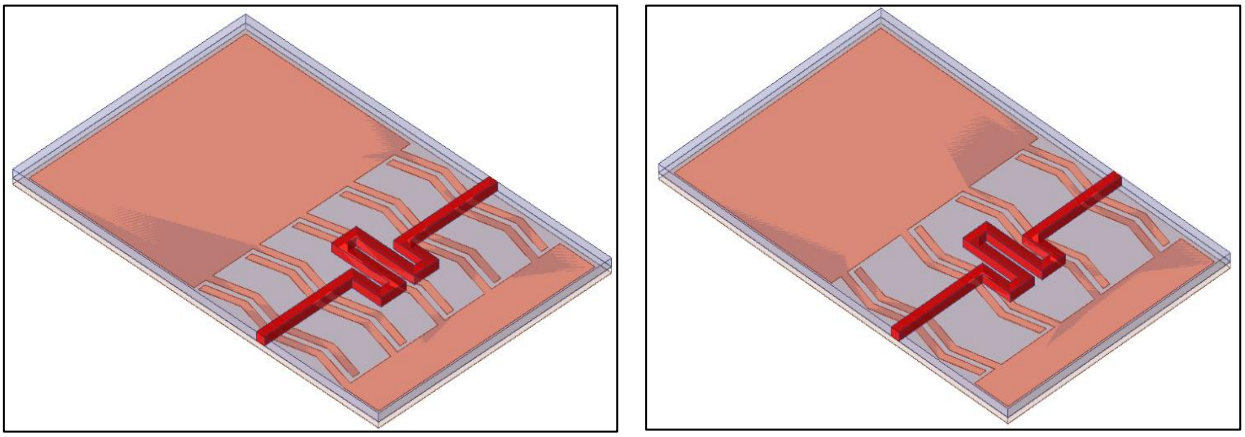

(a) (b)

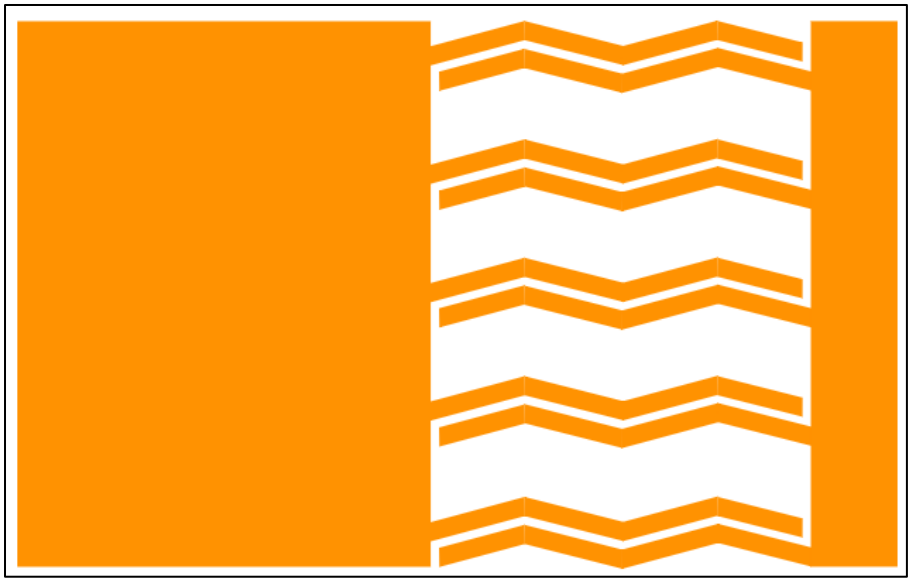

(c)

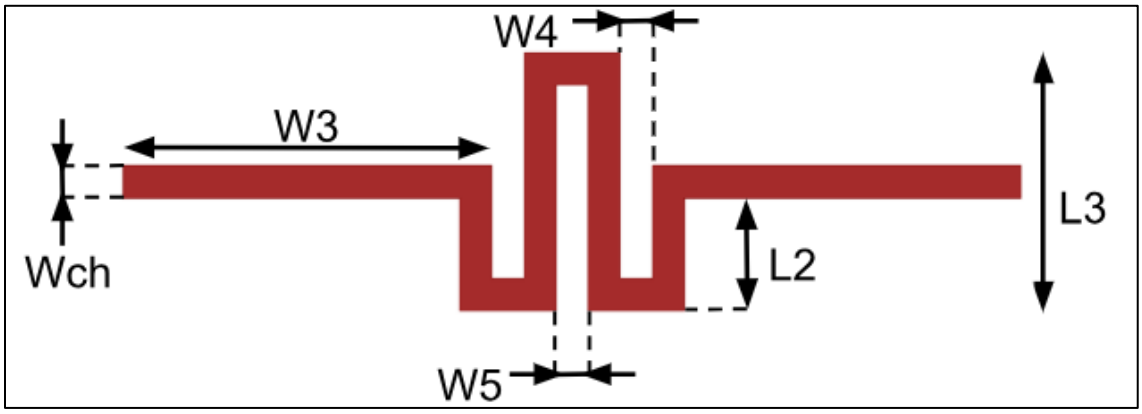

(d)

Fig. 3.12 (a) AMC Unit Cell with 5 Strips (b) 4 Strips (c) Optimised AMC Unit Cell

(d) Optimised Channel dimensions

Fig. 3.13 (a) and (b) show the simulation results of the optimised AMC unit cell. The AMC shows switching from 2.5 to 1.6 GHz and the 0° phase frequency is close to the resonance frequency for both cases. The completion of unit cell optimization brings the design to its final step where the antenna can now be integrated with a mesh of AMC cells.

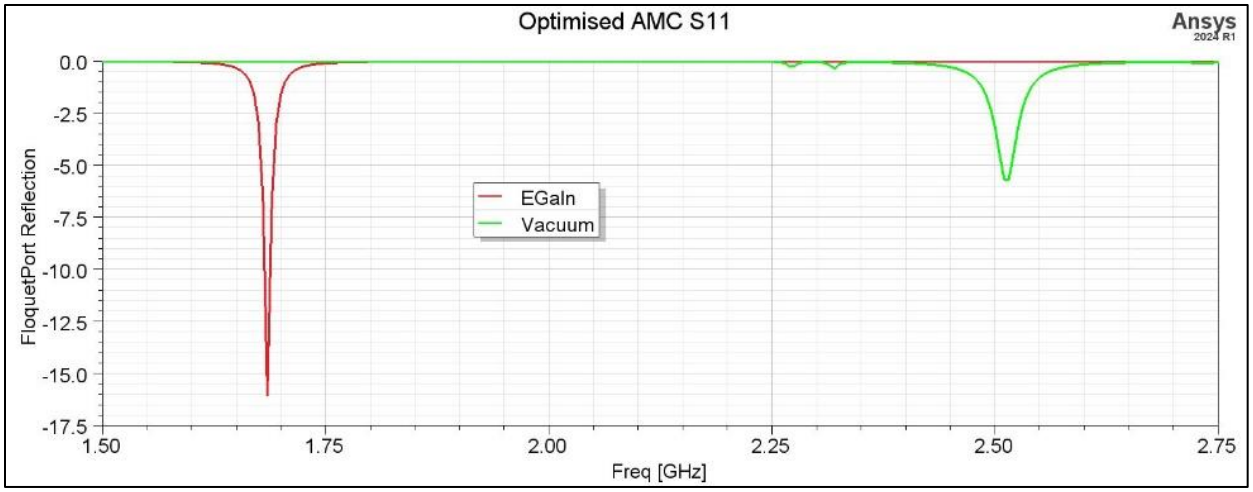

(a)

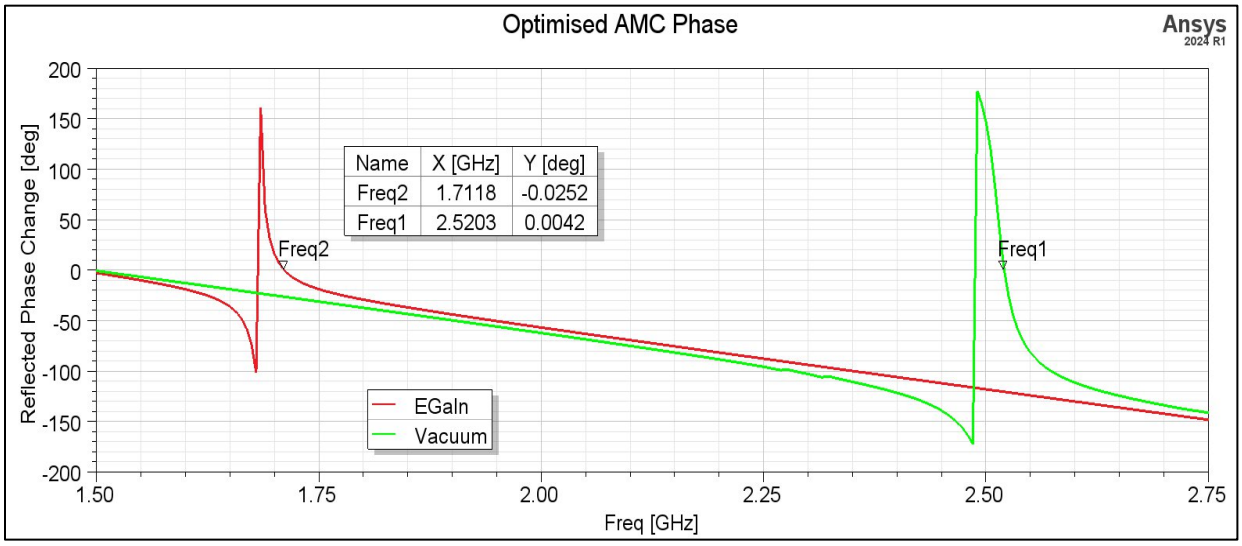

(b)

Fig. 3.13 Optimised AMC Unit Cell (a) Floquet Port Reflection (b) Phase Response

The antenna design with the AMC structure integrated underneath it is shown in Fig. 3.14 (a). The gain of the system with different separation distances, shown in Fig. 3.14 (b), is used to find that a separation of ~2.4 mm between the antenna and AMC as ideal. This separation is then filled with the acrylic substrate of adequate height to achieve the gain values shown in Fig. 3.14 (c) for vacuum and Fig. 3.14 (d) for the EGaIn channel.

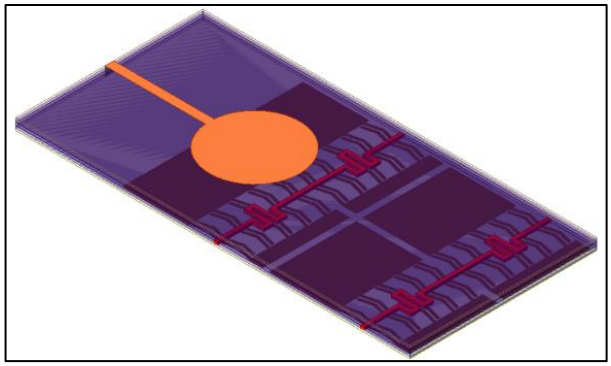

(a)

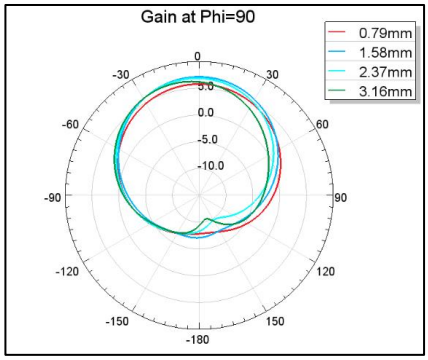

(b)

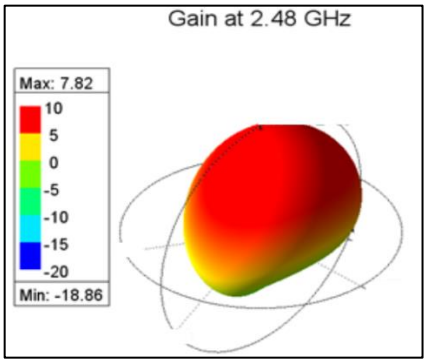

(c)

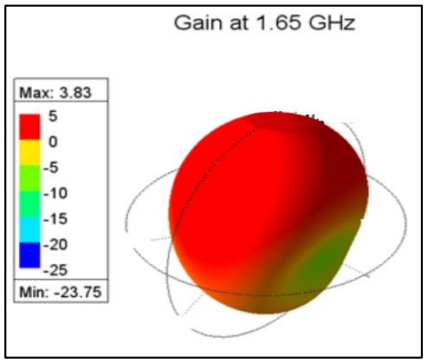

(d)

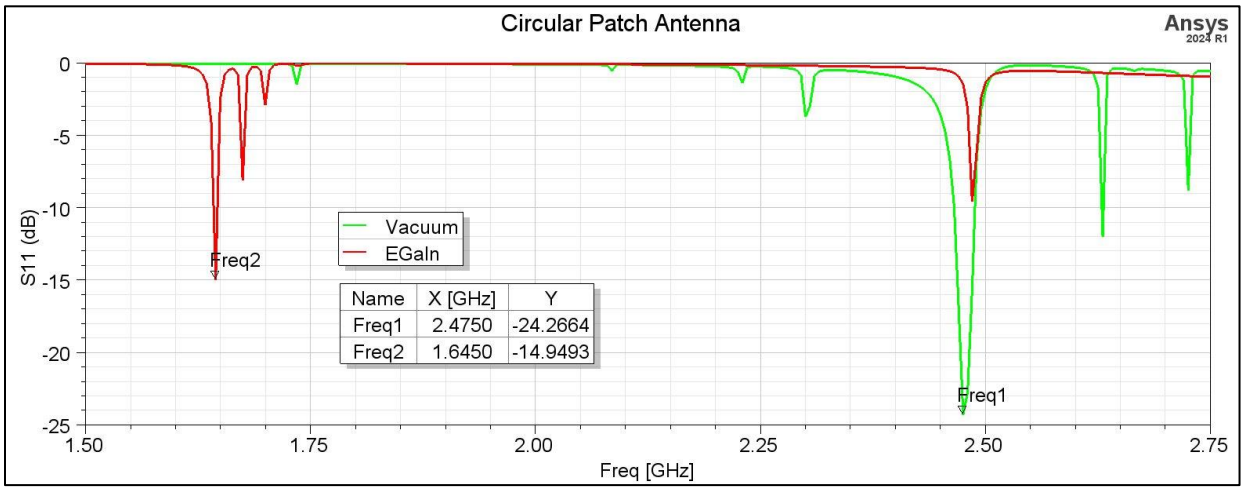

(e)

Fig. 3.14 (a) Optimised Final Design (b) Gain with Different Separation (c) Gain at 1.65 GHz

(d) Gain at 2.48 GHz (e) S_{11} of Optimized Design

It is of great importance to observe that the gain enhancement is achieved due to AMC for both cases, albeit a lower gain is achieved once the antenna has been tuned to 1.6 GHz. This is not surprising as the antenna aperture is optimized for the higher frequency band thus providing efficient radiation performance. Although the gain in the lower band is still in the acceptable range and can be classified as satisfactory for a reconfigurable antenna system. The impedance performance is added in Fig. 3.14 (e) highlighting good matching conditions for both antenna states. The final dimensions of this antenna design are listed in Table 3-2

Table 3-2 Dimensions of Optimized Frequency Switchable Design

Variable	Value (mm)	Variable	Value (mm)	Variable	Value (mm)	Variable	Value (mm)
Lf	30	**W1**	19.8	**Wcp**	0.4	**W4**	1
Lg	24	**W2**	4.2	**Wc**	0.8	**W5**	1
Rp	27	**Lc**	1.96	**Wic**	0.6	**L2**	3.5
Wf	2.6	**Lic**	2.3	**Wch**	1	**L3**	8
W0	18	**L1**	7	**W3**	5.5		

3.4 Conclusion

The impedance switching of a circular patch antenna using liquid metal channels is demonstrated. The design employs an artificial magnetic conductor with a switchable function coming from optimally placed EGaIn channels. With vacuum channels, the AMC shows a gain of 7.5 dBi at 2.48 GHz and with EGaIn channels, a gain of 3.83 dBi at 1.65 GHz. The switchable AMC increases the original monopole antenna's gain by 3 dBi for a vacuum channel and by 1.5 dBi for a LM channel. The patch antenna shows good matching for both operating frequencies and the usage of EGaIn in the design offers a novel method to achieve frequency switching.

CHAPTER 4: POLARIZATION RECONFIGURABLE ANTENNA

The impedance switching design presented in the earlier section achieved reconfiguration by switching between two channel states. This means that the antenna in that case can be selectively tuned to two different operating frequency. In the scope of frequency tunable antennas, this is not a very attractive design. Tuning of frequency would generally entail the movement of antenna impedance continuously within a frequency band. Therefore, the presented solution may not be the most popular one. In fact, a more relevant antenna characteristic that is more suited to step tuning is the wave polarization. Therefore, this chapter of the thesis is centered around such a design.

4.1 Overview of Preliminary Design

To demonstrate polarization agility, the design described in this section uses a truncated square patch antenna with strategically placed LM channels, aimed at disturbing the patch currents, shown in Fig. 4.1 (a). Now, it is well-known from the literature and to antenna designers that this is the simplest patch antenna design that introduces circularly polarized radiation from a single feed antenna element. Thus, the reason for choosing

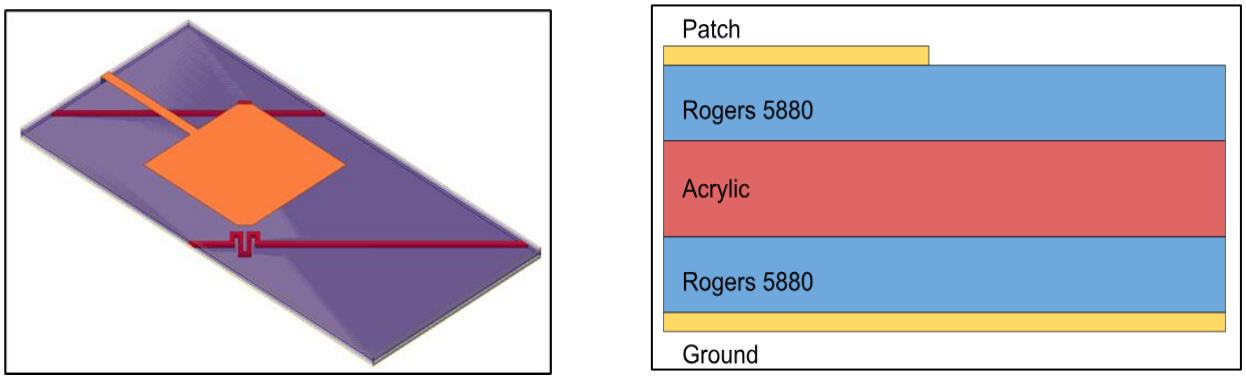

(a) (b)

Fig. 4.1 Polarization Conversion Antenna (a) Preliminary Design (b) Substrate Stackup

this design. While the antenna with vacuum channels is designed to operate with circular polarization at 2.5 GHz, the introduction of EGaIn in the same channel should switch the antenna's polarization to linear without altering the operating frequency or adversely affecting the gain. Thus, realizing a polarization reconfigurable antenna.

The antenna is designed on a similar substrate stack up as is used for the frequency switchable design of the last chapter, Fig. 4.1 (b). At first, the channel shape is reused from the previous design as it avoids introducing new variables. However, two diagonally placed channels that are parallel to each other are used for this design. Each antenna truncation is assigned a channel beneath it to control the electric fields between the antenna and the ground plane. Since the polarization agile antenna needs to show multiple polarization states at the same frequency, the AMC is not required and is excluded from the design. This would simplify the design process and its final implementation during fabrication. The simulation results of the antenna design are discussed in the following sections along with the modifications done to achieve the final optimized results.

4.1.1 Simulation Results of Preliminary Design

A square patch with a length of 27 mm is used as the starting point in this case. Two triangles are truncated from the diagonal edge of the antenna aperture to achieve the stated circular polarization. The area of these truncations is 6.125 mm^2. These types of circularly polarized antennas are well-known in the antenna community and are explained in detail in antenna textbooks [1]. Therefore, it is prudent to skip this part of design. The antenna is fed with a microstrip line but with minimized length of 5 mm. The length of the line is intentionally kept small to determine the antenna impedance at its edge. It should

be reminded here, that for a truncated patch antenna inset feeding technique is not usable. Inset feed disturbs the field pattern underneath a patch antenna, which works fine in the case of linear polarization but is not a viable option for a circularly polarized design. The dimensions of the antenna are defined as variables in the simulator as shown in Fig. 4.2 (b). This is done in anticipation that a parametric study for such a design is almost inevitable.

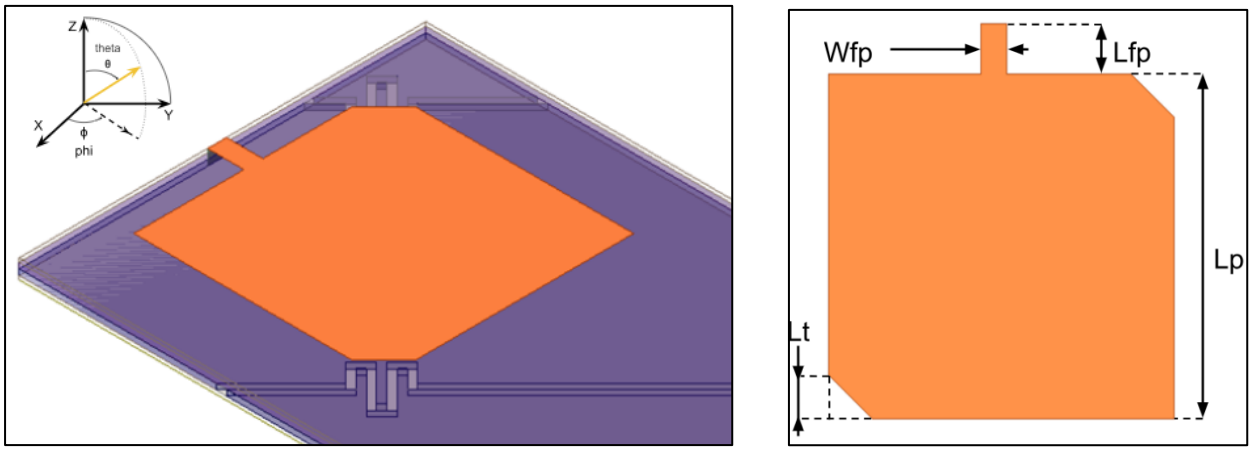

(a) (b)

Fig. 4.2 (a) Simulation Model for Truncation Parametric Analysis

(b) Truncated Patch Antenna Dimensions

The impedance matching of the initial design with both the vacuum and EGaIn channels are shown in Fig. 4.3 (a). With the vacuum channel, the antenna has an S_{11} response of -5.9 dB at 2.5 GHz which shifts to a lower frequency of ~2.4 GHz due to the introduction of EGaIn inside the channels. This type of result is not conducive to polarization reconfigurable antenna as the designer would like to see the operation at the same frequency without any tuning, thus the antenna result needs some optimization. Moreover, Fig 4.3 (b) shows the AR with both the channels and offers insight into the

polarization behaviour after the switching process. As seen from marker M1, the vacuum filled channel results in the antenna having an AR of 9 dB indicating poor circular polarization. However, with EGaIn channels, the AR increases to 16 dB. While this alone does not confirm linear polarization, the increased AR confirms that the EGaIn channels can influence antenna polarization by disturbing its field beneath. Simulation results from

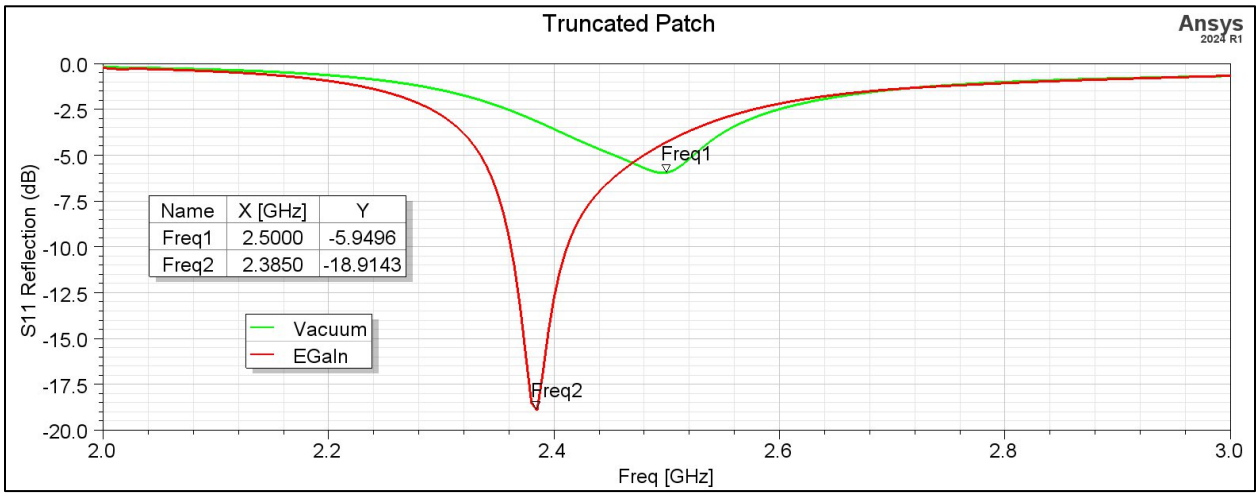

(a)

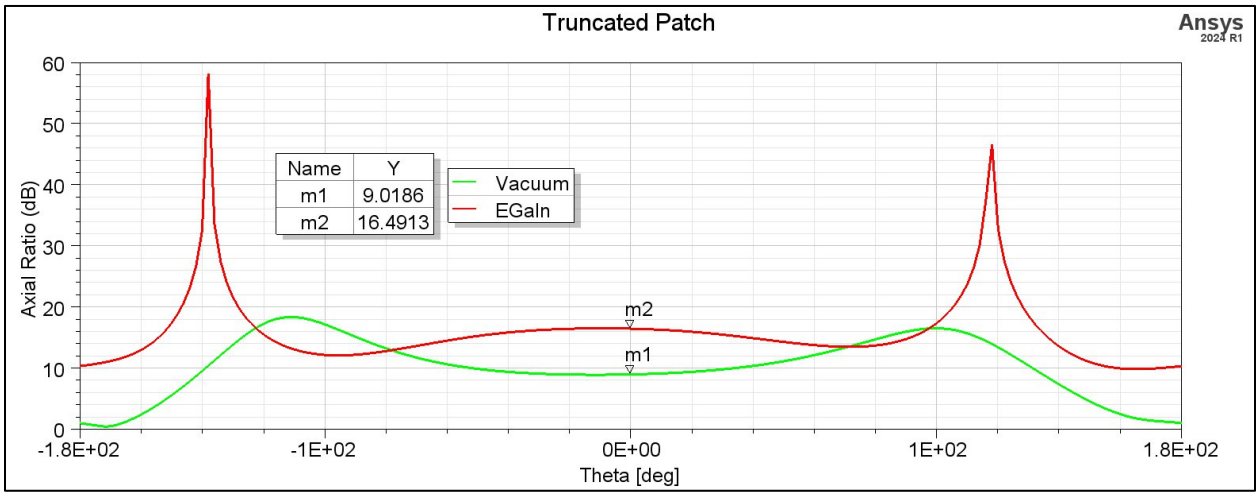

(a)

Fig. 4.3 Preliminary Design (a) S11 Response (b) Axial Ratio

the preliminary design reveals that while the introduction of EGaIn is producing a noticeable change in polarization, this change is also accompanied with a shift in operational frequency.

This shift is reduced in the final design through studying the shape and placement of the EGaIn channels. Furthermore, an antenna is considered circularly polarized with an AR below 3 dB and linearly polarized if the co-polarization is larger (typically 15 dB or more) than the cross-polarization. The latter result would result in AR values of more than 10 dB or so. Thus, there are a series of steps that need to be carried out for this design to operate as intended. The goal is that the final design works as a linearly polarized antenna with the vacuum channels and switches to circularly polarized one when EGaIn is introduced into these channels. Moreover, the frequency of operation needs to be same for both these cases.

4.2 Antenna Design Optimisation

4.2.1 Parametric Analysis of Truncated Patch

The truncation of the patch antenna mainly influences its polarization of radiation. Therefore, a parametric analysis is studied on the length of the patch antenna truncation, 'L_t', as the starting point. As the polarization is very sensitive to variations in L_t, the feed of the antenna is kept at a minimum for simplicity. Fig. 4.4 provides the axial ratio for different values of L_t. At the boresight of radiation (i.e., $\theta = 0°$), the value of AR is preferred to be below 3dB as this is the point of maximum antenna gain. Keeping antenna impedance and gain in mind, a CP antenna with truncation size of L_t*=4.3 mm* is chosen despite the antenna not being impedance matched. This is mainly due to the shortened

feed and will be alleviated by designing a better matching network. Thus, the focus is kept on radiation performance more than the antenna impedance which can be looked into at a later stage. The antenna length 'L_p' also helps in try to achieve the sweet spot for the AR value. However, between the two variables, the former i.e., L_t plays a more dominant role. Hence, the rationale of keeping the focus of discussion on it. The antenna with its optimized AR value provides a stable gain of 7.14 dBi at 2.5 GHz. Now, the focus can be turned to the impedance of the antenna.

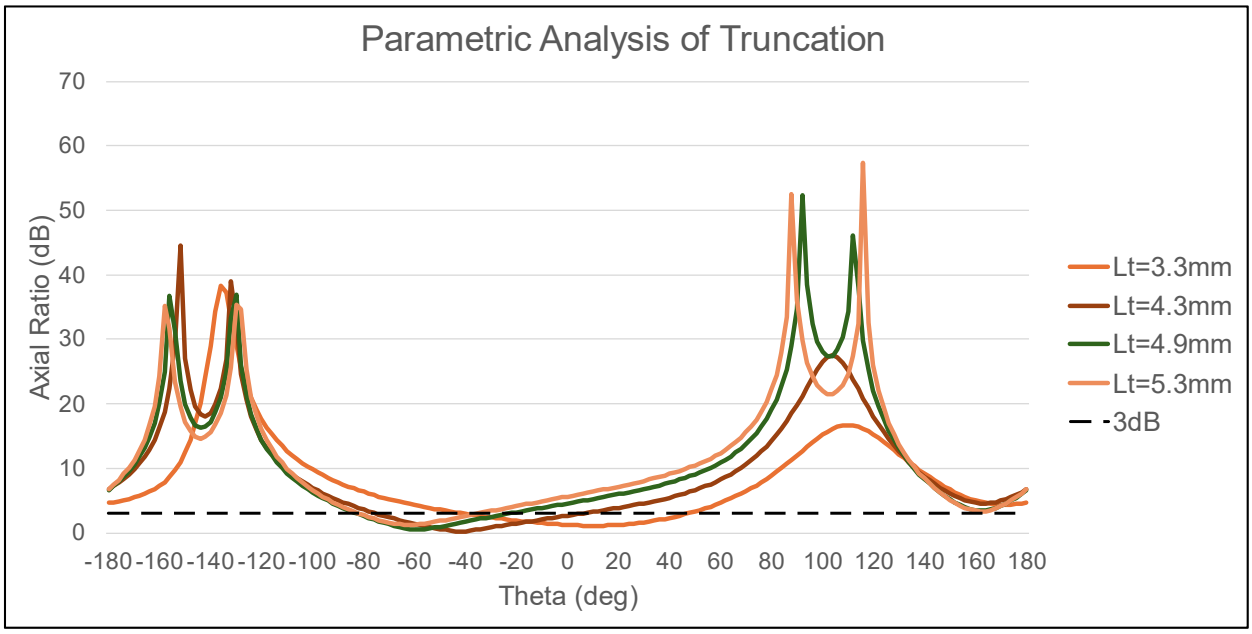

Fig. 4.4 Parametric Analysis of Truncation

4.2.2 Impedance Matching of the Design

A shunt stub is a common method to achieve better matching and works extremely well when the load has a combination of real and imaginary impedance, shown in Fig. 4.5 (b). It could be open circuited or short circuited on its edge. Here, open circuited is chosen as the preferred candidate just because its ease of realization. Beyond the open stub on the feed, a smaller extension of the feed is provided to mount an SMA connector.

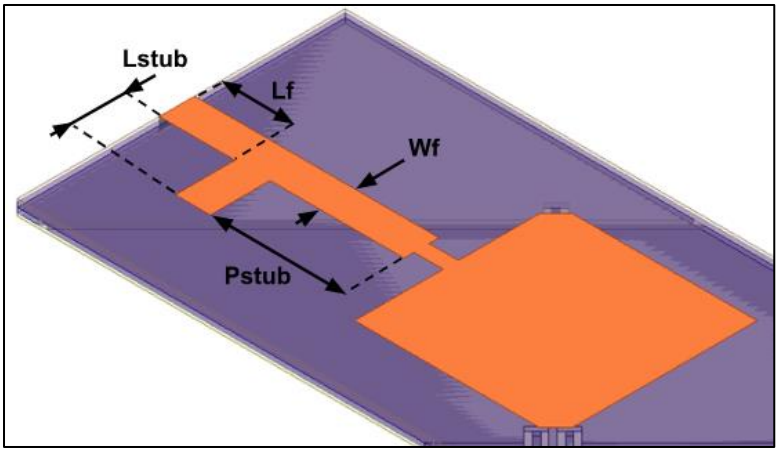

(a)

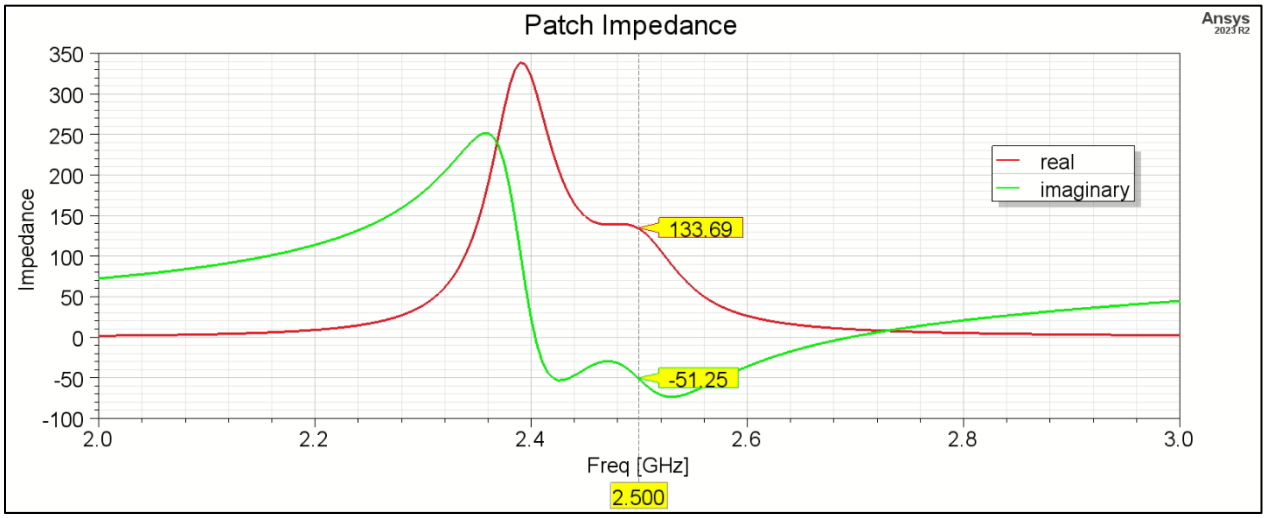

(b)

Fig. 4.5 (a) Impedance of Truncated Patch (b) Feed Dimensions

The antenna feed's dimensions are chosen through simultaneous parametric analysis of the stub position P_{stub} and length L_{stub}. While the position of the stub brings the feed's resistance closer to 50 Ohms (intended value), the stub length tries to reduce the imaginary impedance of the antenna [1]. The width of the microstrip line W_f is calculated using standard methods for microstrip line. This is a parameter which does not have a lot of range and thus cannot be considered as one of the variables. The parametric analysis

on the length, L_{stub} and position, P_{stub} of the stub shows multiple combinations of the two variables that produce the required matching. Among many others, Fig. 4.6 only shows the S_{11} results of one stub position with varying stub lengths. It can be seen that for the combinations L_{stub} = 7.8 mm and P_{stub} = 22.9 mm and L_{stub} = 9.6 mm and P_{stub} = 22.9 mm, the antenna achieves the desired results. This is anticipated and is the prescribed target of this optimization. However, despite not changing the truncation L_t, the introduction of the open stub inadvertently causes the antenna to lose its circular polarization.

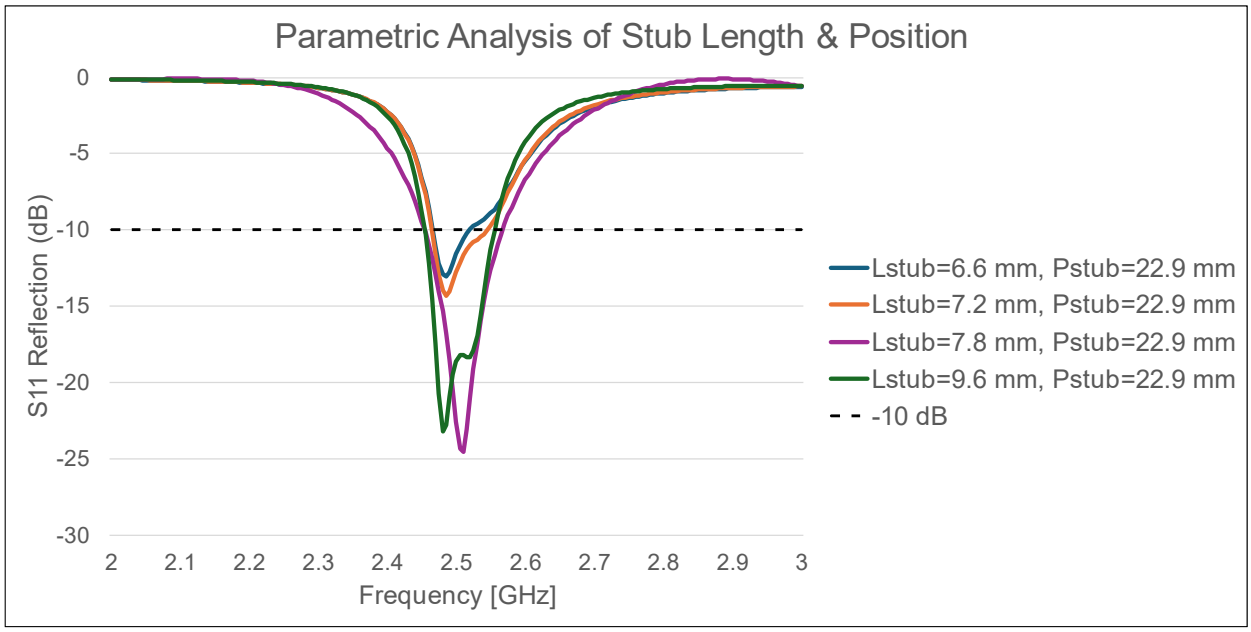

Fig. 4.6 Feed Network Parametric Analysis

This required another series of simulations on the antenna dimensions, i.e. length and the truncations to be optimized. For sake of conciseness these steps are overlooked here since they have already been covered in the last sub-section. The optimised vacuum antenna shows good matching at the target frequency, Fig. 4.7 (a), and a low axial ratio of 1.4 dB maintaining circular polarization, Fig. 4.7 (b). Table 4.1 provides the dimensions of the optimised patch and the matching network.

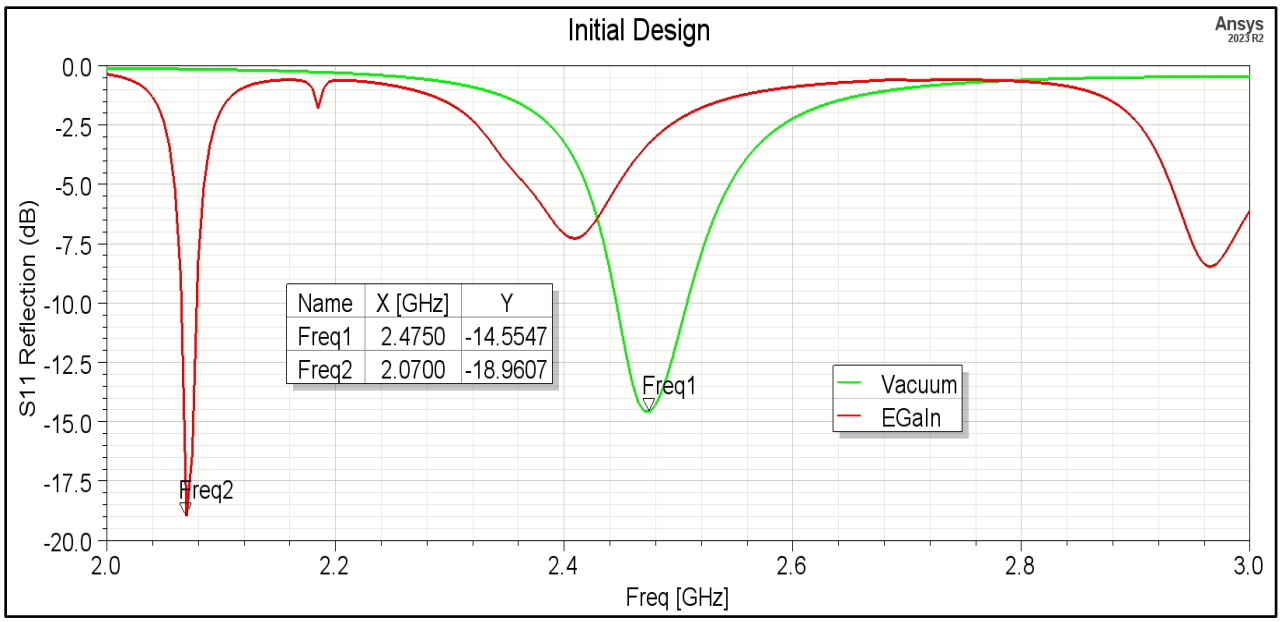

(a)

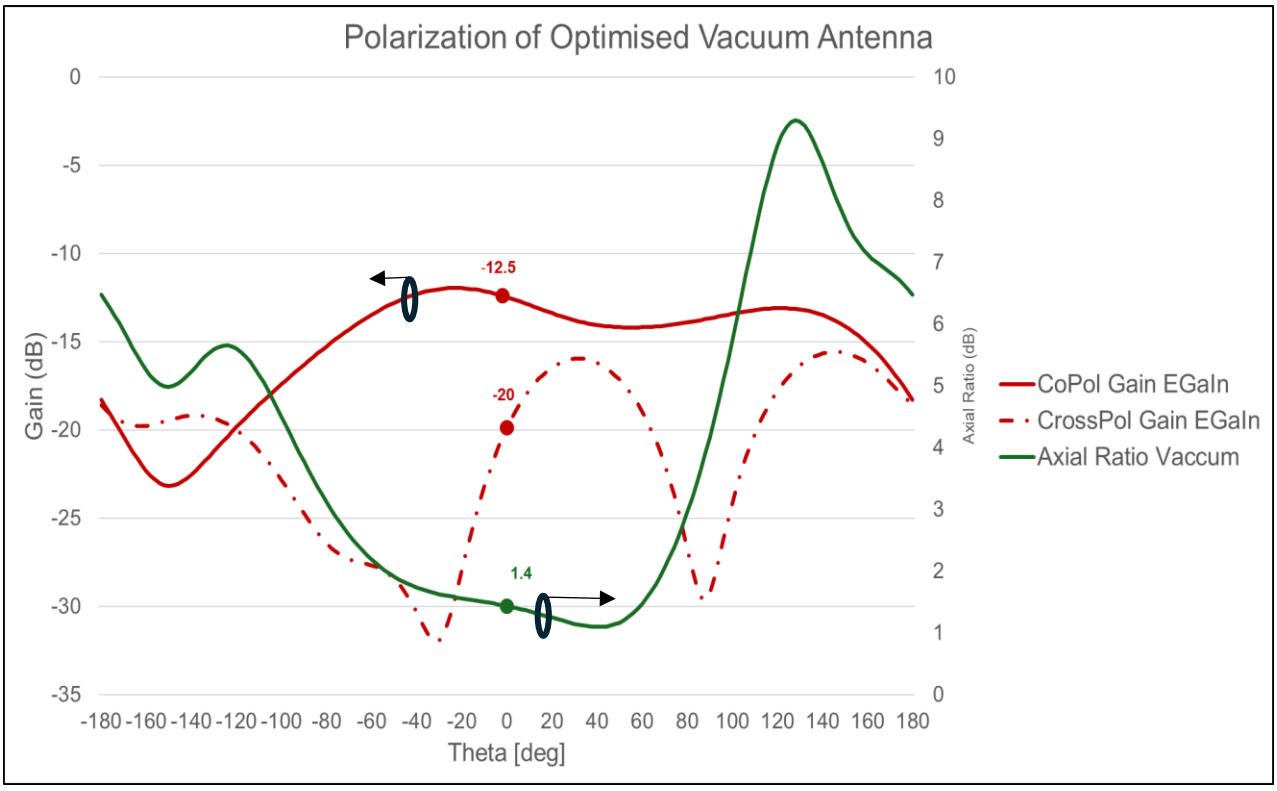

(b)

Fig. 4.7 Optimised Vacuum Antenna (a) S11 Response (b) Polarization Results

Achieving the results with the vacuum channels, meant to observe the antenna results in the presence of EGaIn underneath. Not to author' surprise, the antenna with EGaIn in the channels is not working as intended. Firstly, the EGaIn antenna does not show a 15 dB difference between the co-polarized and cross-polarized gain which is the requirement to achieve linear polarization. Furthermore, Fig. 4.7 (a) also shows that with the insertion of EGaIn into the channels, the frequency downshift mentioned in section 4.1.2 is still present. Despite these issues, the decreased gain of the cross-polarized radiation indicates some loss of circular current on the patch. Therefore, it is a positive sign and indicates that the channels with EGaIn could switch the antenna polarization to linear.

Table 4-1 Dimensions of Optimized Frequency Switchable Design

Variable	Value (mm)	Variable	Value (mm)
L_p	34.2	P_{stub}	21.2
L_t	3.5	L_{stub}	11.9
L_{fp}	5	W_f	6
W_{fp}	2.6	L_f	12.9

4.3 Analysis of EGaIn Channel

4.3.1 Surface Current on Liquid Metal Channels

Before optimizing the antenna results in the presence of the LM i.e., EGaIn in the channels, it is important to understand as to why the change is happening when the channel is switched from vacuum to metal. The reconfiguration in this design is achieved by disturbing the patch currents with the help of the acrylic channels. These currents, in turn effect the antenna electric field within the substrate thus causing a change in the radiation characteristics. As seen in the previous section, there is already a small reduction in circular radiation when the EGaIn is introduced into the channels. This is attributed to the high conductivity of the LM and can be utilized to have a larger impact

on the antenna. However, this excellent conductivity is also causing the antenna to shift to a lower operating frequency and the simulation results with EGaIn inside the channels provides an explanation for this. Since the optimised CP patch has two truncations, the design contained two channels underneath the antenna, one for each truncation. However, the current distribution on the bottom of the EGaIn channel, Fig. 4.8 (a), shows that each channel behaves slightly differently. While channel 1 shows minimal current that is based on the distance from the truncation, channel 2 shows large current positioned closer to the matching network rather than the truncation. Therefore, the unnecessary frequency switch is due to the interactions between these currents and the matching network. This led to the next step of investigation where channel 2 is removed from the design. The analysis explained in this section and its consequent result shown in Fig. 4.8 (b) indeed proves that the channel 2 is causing the unnecessary shift and can be eliminated from the design altogether.

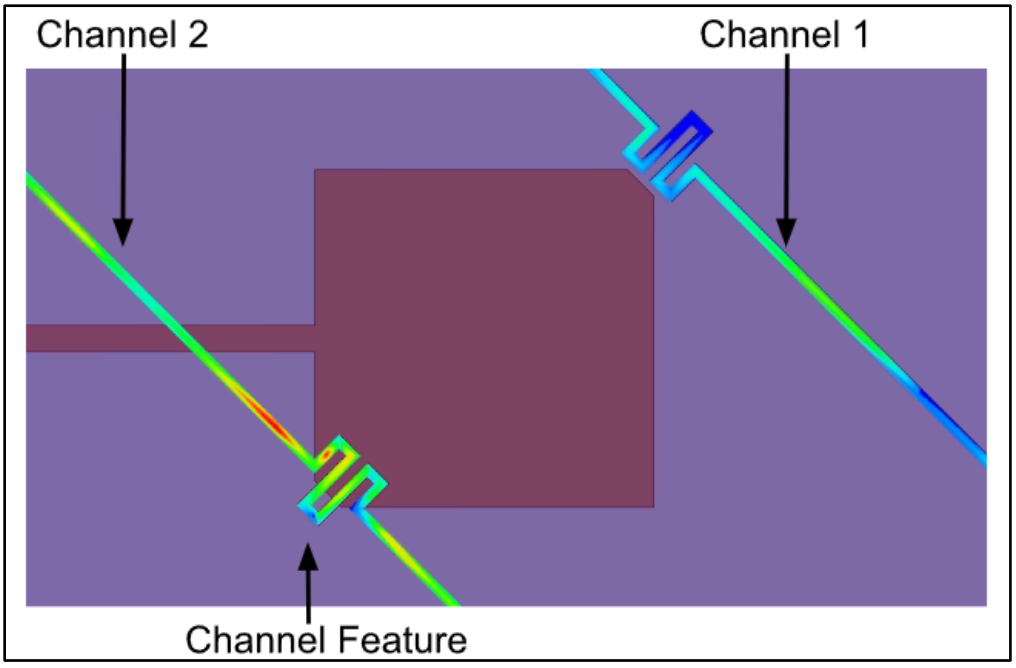

(a)

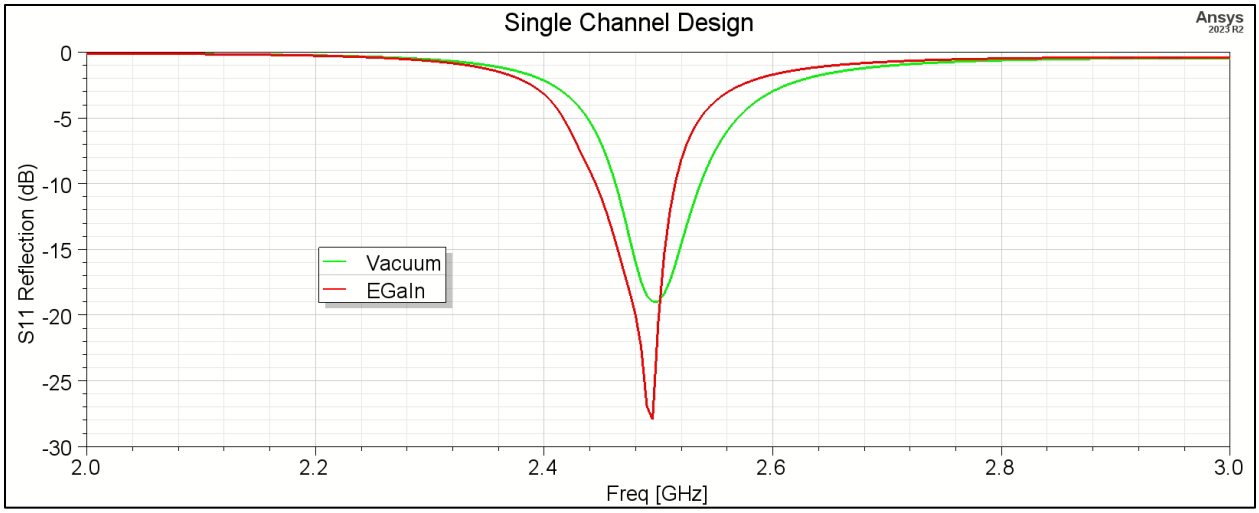

(b)

Fig. 4.8 Vacuum Optimised Antenna (a) Surface Current (b) S11 Response with Single Channel

While the antenna can function at the same operational frequency for both vacuum and EGaIn channels, the LM state still does not show significant linear polarization due to the minimal interaction between the patch and the remaining channel. The circular polarization of the vacuum state is still maintained. Thus, the focus can be reverted to the case when EGaIn is present inside the acrylic channels.

4.3.2 Influence of Channel Shape & Placement

The first idea that comes to mind for this optimization is the channel shape and its placement underneath the antenna. Both these parameters are expected to have minimal effect on the circularly polarized antenna (i.e. the one with the vacuum), because of absence of any significant material inside the channel. The parametric analysis of truncation length, L_t in section 4.2.1 revealed that the circular current is easily disturbed when the channel is in closer proximity to the truncated area. This is due to the presence of impinged currents on the channel metal due to the antenna radiation. The stronger the

currents in the channel, the more their effect would be on the antenna performance. A closer look at the current distribution within the channel shows that most of the current is not over the channel feature. Instead, the shape of the channel feature provides a greater impedance than the straighter portion of the channel, resulting in the current being isolated over the straight segment just outside the channel feature. This effect can be seen in Fig. 4.8 (a) where the magnitude of the current is significantly larger outside the spiral shape of the channel. This shows that a better interaction between the antenna and the channel can be achieved by better placement of the latter. Therefore, both the channel design and placement are studied in this section for improved antenna performance.

The goal in redesigning the channel shape is to be able to control the location of the current over the channel. Like conventional circuits, the current over the EGaIn surface prefer paths of lower impedance and channel features with increased intricacy are used to have better control over the flow. Different channel features with varying degrees of complexity are designed and simulated, few of which are presented here. For example, type 1 is a simple cuboid which distributes current more evenly across its surface, Fig. 4.9 (a). Therefore, the magnitude of the current near the truncation is small, and the cross-polarized gain is not reducing enough, Fig. 4.9 (d). On the other hand, type 2 has a triangular structure and much less even distribution of surface current, Fig 4.9 (b). There is a larger build-up of current outside type 2 and interactions with the truncation is strong causing a significant change in antenna polarization. While type 2 can achieve LP, it comes at the cost of antenna matching. Drastic changes in the feature's structure interact in different ways with the fringe fields undeath the antenna and completely alter the patch current. Therefore, type 2 is not chosen for this antenna design. Type 3, on the other

hand, contains a smaller profile but retains the triangular shape from type 2. It also contains cutouts to reduce the surface area inside the feature and help in isolating more current outside. The antenna with type 3 is well matched at the design frequency but does not produce a 15 dB separation between cross and co-polarized gain to achieve the desired linear polarization.

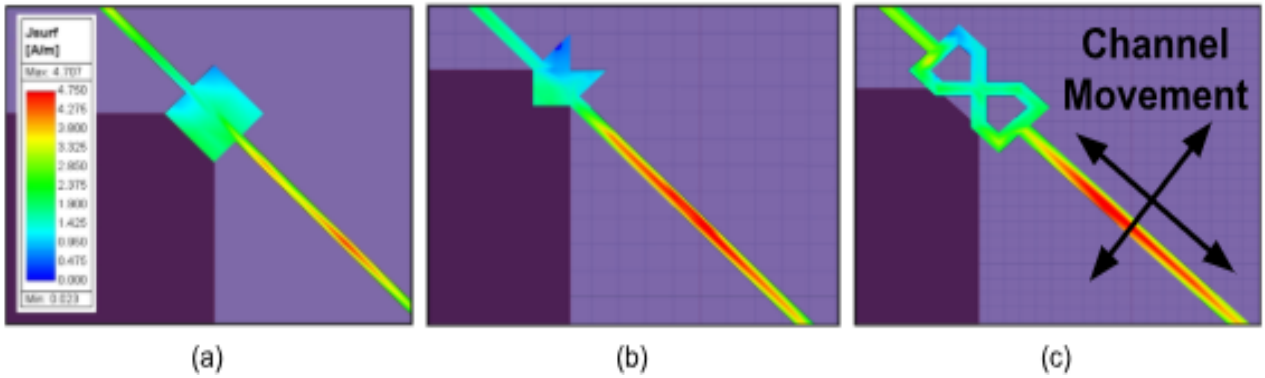

(a) (b) (c)

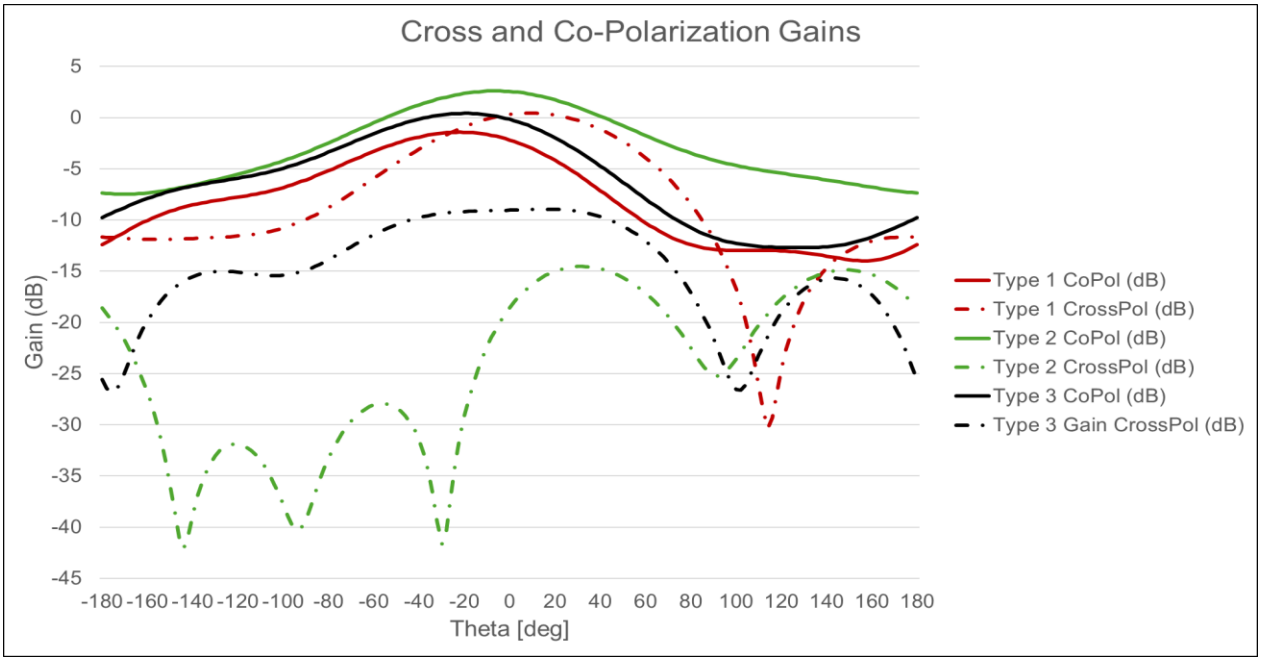

(d)

Fig. 4.9 Surface Current on Channel Features (a) Type 1 (b) Type 2 (c) Type 3

(d) Gain Response of Different Channel Variants

The cross polarized gain can be reduced by further increasing the interaction between the patch and the channel. This is achieved by moving the point of maximum current closer to the truncation. The feature is moved relative to the patch and an increase in axial ratio is observed at a specific position. At this position, the circular current on the patch is directly impeded by the channel and causes a dramatic change in AR, Fig 4.10.

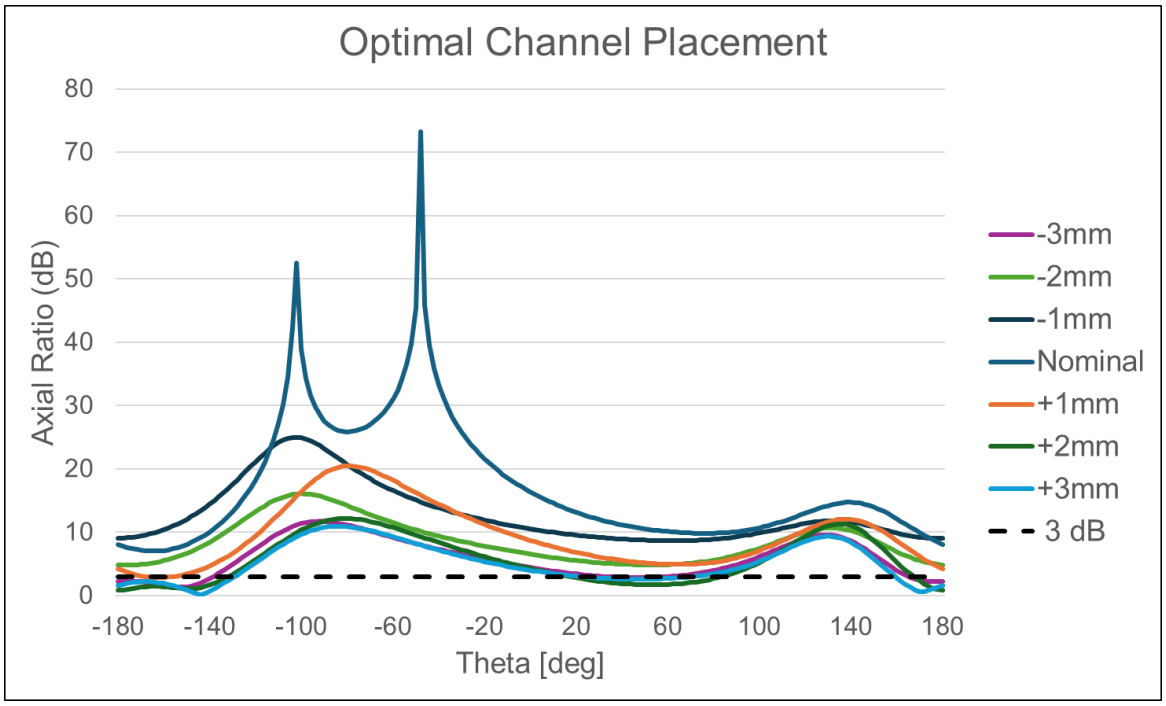

Fig. 4.10 Axial Ratio for Different Channen Placements

These series of steps, fortunately, provide the desired results where the antenna is able to switch its polarization at the same operating frequency for two cases of acrylic channels. However, it is observed that the design is very sensitive to the channel placement and a small variation could cause a significant change in the antenna radiation performance. Hence, a better channel design is needed to cater for this downside. The author came up with the one shown in Fig. 4.11. It consists of two identical features one to be placed on either side of the truncation that would result in building up of large

currents in-between them (i.e., the section labelled as L4). Changing the distance of the channel features from the truncation produces results like Fig 4.10 but the design has significantly lowered sensitivity. The dimensions of the optimised channel feature are listed in Table 4-2 and the next section covers the performance of the CP antenna with the channels underneath.

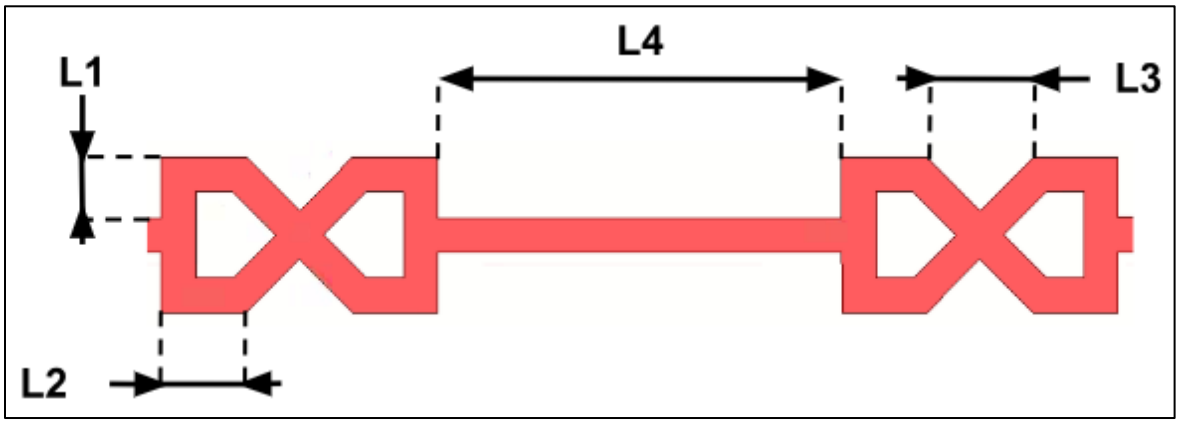

Fig. 4.11 Optimised EGaIn Channel Feature Dimension

Table 4-2 Dimensions of Optimised EGaIn Channel

Variable	Value (mm)
L_1	1.76
L_2	2.5
L_3	3
L_4	12

4.4 Optimised Polarization Reconfigurable Design

The truncations in section 4.2.2 produces circular polarization and the optimised channel described above is designed to suppress the effect of this truncation. The new channel design is modeled within an acrylic substrate and the material assignment is changed to EGaIn to simulate the switching of operational states, Fig. 4.12 (a). The optimised channel in the EGaIn state shows an S11 of ~-11 dB at 2.5 GHz, Fig. 4.12 (b). Like the analysis

around channel placement in section 4.3.2, the precise placement in this design can also be changed to improve the matching. However, a trade- off between S_{11} and co-polarized gain is achieved in this design where the antenna can show linear polarization while maintaining the best-case matching. The EGaIn state shows linear polarization through the required 15 dB separation between cross and co-polarized gain, Fig. 4.13. This is further verified by plotting RHCP and LHCP radiations for the EGaIn state. It is quite obvious that both these radiation levels are almost equal to each other emphasizing a linear polarization from the design in the presence of LM in the channel.

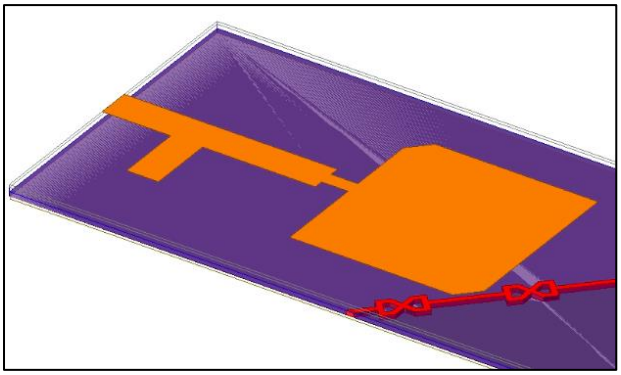

(a)

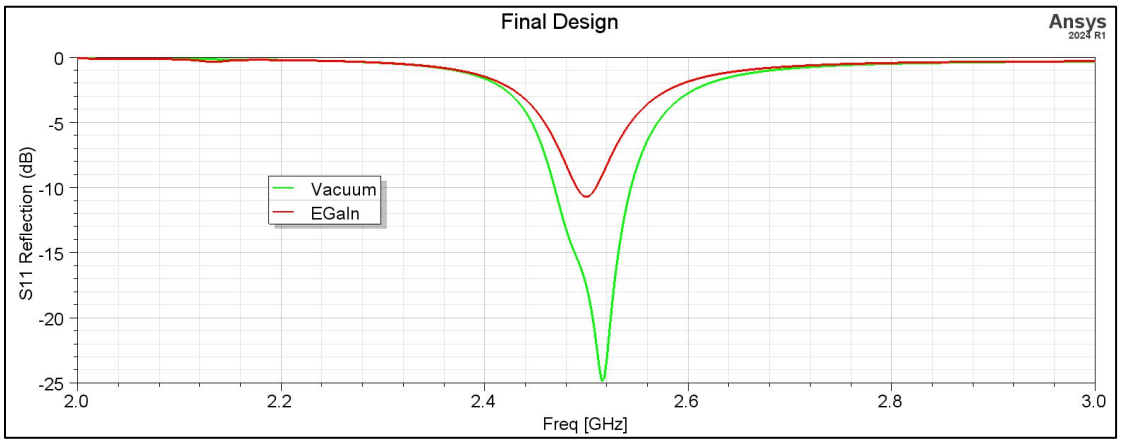

(b)

Fig. 4.12 Polarization Switchable Design (a) Showing channel placement (b) S11 Response

To theoretically, understand the change in the antenna polarization in the presence and absence of the LM in the acrylic channel, it is interesting to study the surface currents on the patch structure, Fig. 4.14. The antenna is initially designed to provide RHCP radiation by placing the truncations on the edges a specified before, (truncations can be seen in Fig. 4.5 (a)). This selection is entirely arbitrary as it does not affect the illustration of the concept. By switching the position of the truncations to the other diagonal, would cause it to radiate an LHCP radiation. The point of interest of plotting the currents on the patch structure is to show the trend that they follow. Although this explanation would be more clear in a video, a pictorial representation still labours the point. Fig. 4.14 (a) shows that the current on the patch is not following a straight line and is rather showing a curl in its motion. As seen on the simulator, it shows a circular path followed by the current on the patch surface, resulting in an axial ratio value of less than 3dB.

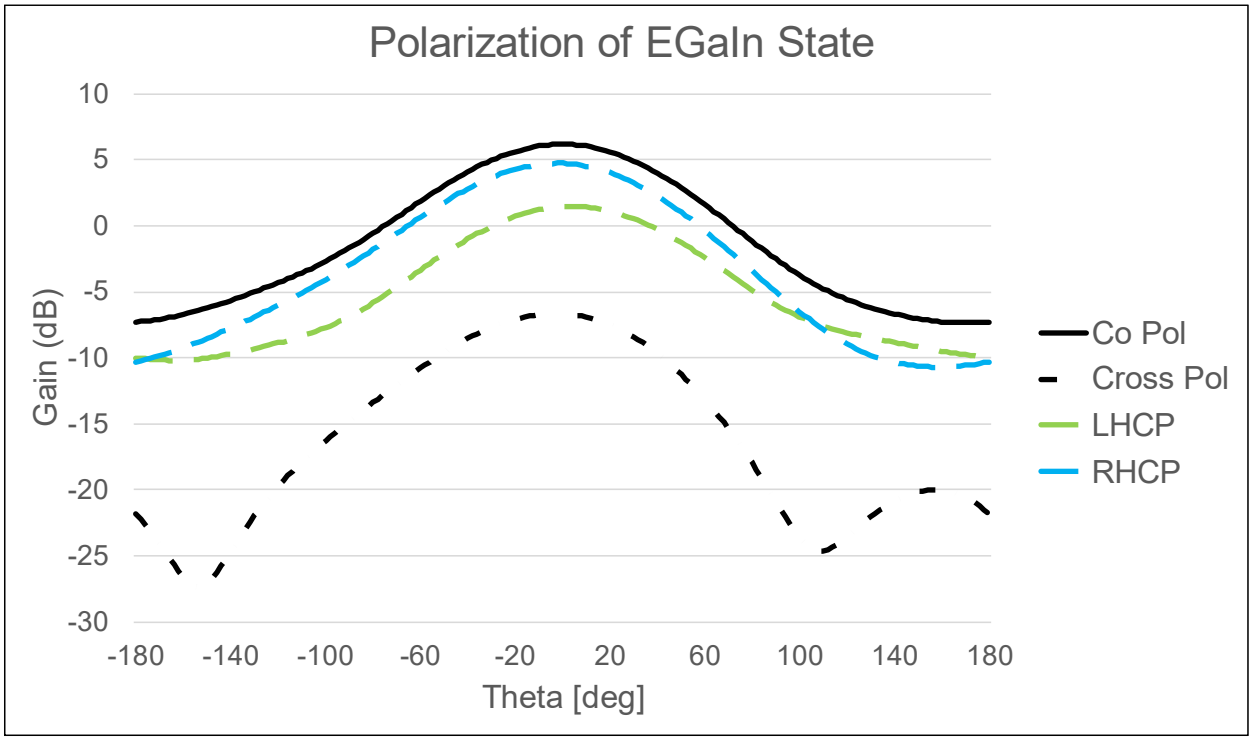

Fig. 4.13 Gain Response of EGaIn State

As opposed to this, in Fig. 4.14 (b) the currents stay linear flowing from one radiating edge of the patch to the other without any curling behavior. This results in a linear polarization from the radiator. Fig. 4.14 (a) shows the case where no metal is present in the channel (i.e., vacuum case) while Fig. 4.14 (b) is the case when EGaIn has been filled in the channel. This analysis provides an analytical explanation to the change in the antenna polarization in the presence and absence of LM.

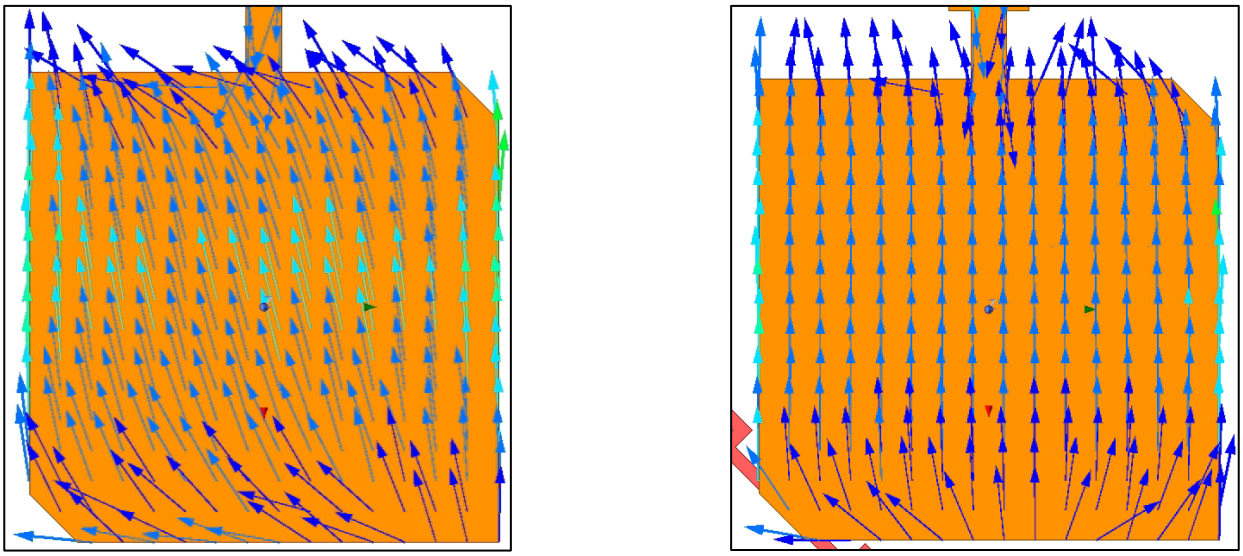

(a) (b)

Fig. 4.14 Surface Current of Patch (a) Vacuum State (b) EGaIn State

4.5 Polarization Versatile Design

With the design that is presented in the last section, leads to a point where one would like to have a single antenna system that can produce all three polarizations, i.e., linear, LHCP and RHCP. It is well-known that a linear polarization is combination of LHCP and RHCP radiations. Thus, if the design has both polarizations simultaneously then effectively it would radiate a linear wave. Therefore, a double truncated patch that can produce linear polarization is used in the polarization versatile design. Two channels that are mirror

image of each other are modeled with underneath the antenna as shown in Fig. 4.15. The concept here is that when one of the channels has EGaIn filled in it, that would result in one type of circular polarization. For instance, if channel 1 has LM filled in it, it would cause a disturbance to the RHCP radiation resulting in an LHCP wave coming out of this antenna. Likewise, RHCP wave can be generated from the same design by switching the presence of LM in channel 2. When both the channels are empty, the antenna would be radiating with linear characteristics. In Fig. 4.15, EGaIn is present in channel 2, while channel 1 is devoid of any metal. The design process detailed in section 4.2 and 4.3 is repeated on the polarization versatile design.

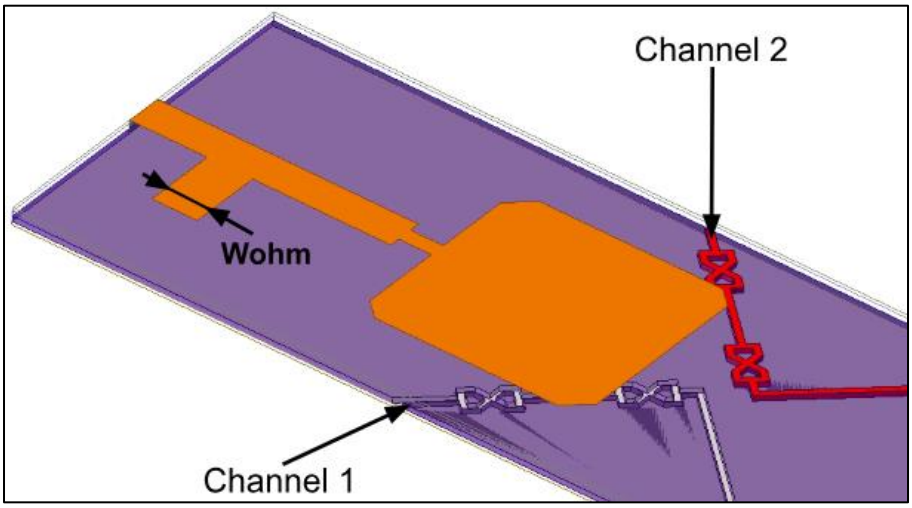

Fig. 4.15 Polarization Agile Design

The 3 states explained above are executed on the antenna of Fig. 4.15 and its impedance results are plotted in Fig. 4.16. The antenna maintains its impedance for all 3 polarizations. It operates at 2.5 GHz with adequate bandwidth. Since this is a reconfigurable antenna, one does not expect it to perform the best in all the cases. However, a minimum criterion needs to be met which is defined as S_{11}<-10 dB. This is clearly achieved in Fig. 4.16.

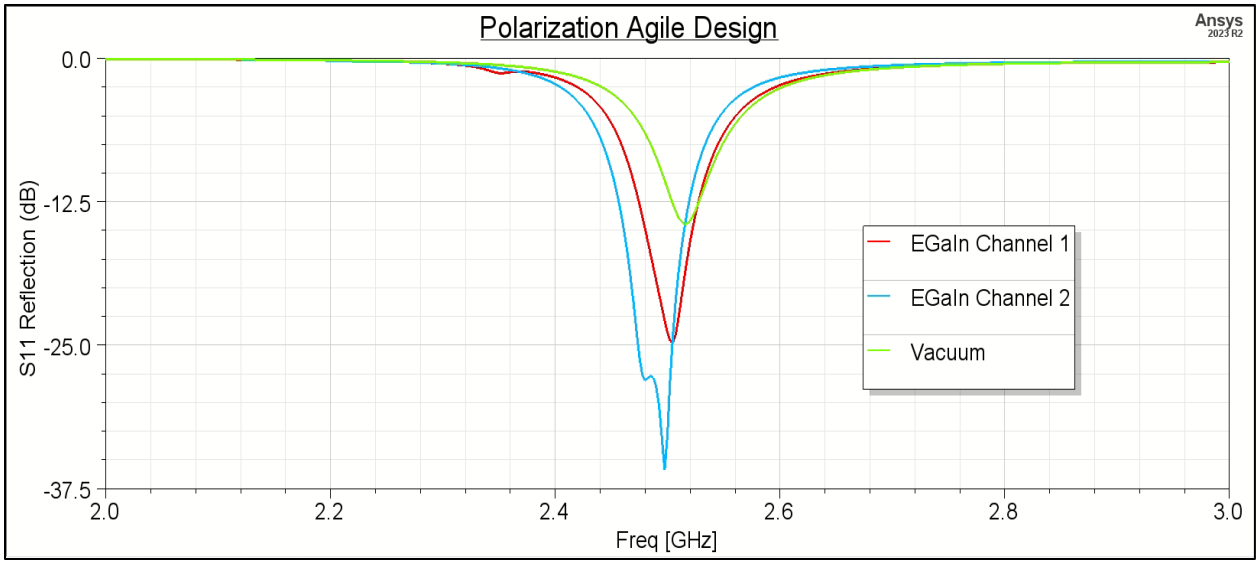

Fig. 4.16 Polarization Agile Design S_{11}

Lastly, it is imperative to see what is happening to antenna's radiation in the 3 states. When EGaIn is present within channel 1, the antenna emits RHCP radiation with an axial ratio of 2 dB and a gain of 7.22 dBi. Alternatively, the presence of EGaIn in channel 2 switches the radiation to LHCP with an axial ratio of 3 dB and a gain of 7.18 dBi. When the channels are empty the value of AR jumps to almost 10 dB outlining a linear case of radiation. Thus, 3 different polarization states are achieved from the design at 2.5 GHz, Fig. 4.17. The patch current moves away from whichever channel contains the EGaIn and in turn produces the two distinct circular polarizations. The sense of rotation of the current for the two cases are exactly opposite, classifying them as two different polarizations although both being circular. The surface currents on the linearly polarized designs have already been covered in the last section. Thus, this final design achieves all the possible polarization for the antenna radiation. It could switch between two circular ones and completely alter to linear radiation if needed. The dimensions of the final optimized design are summarized in Table 4-3.

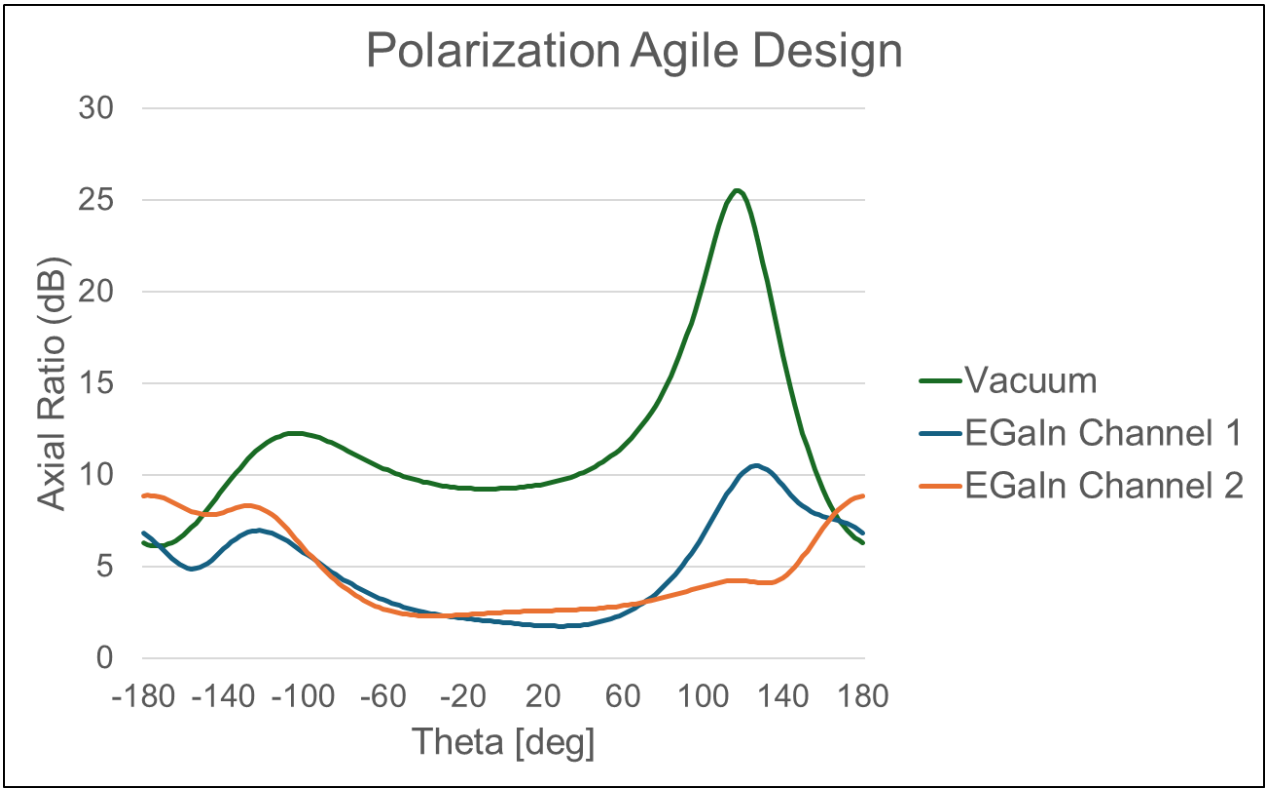

Fig. 4.17 Polarization of Operating States

Table 4-3 Dimensions of Polarization Agile Antenna

Variable	Value (mm)	Variable	Value (mm)	Variable	Value (mm)
L_p	34.2	L_{fp}	5	L_f	11.9
L_t	3.5	W_{fp}	2.6	L_{stub}	11.9
L_{t2}	2.6	P_{stub}	21.2	W_{stub}	7
				W_f	6

4.6 Conclusion

The ability of EGaIn to achieve polarization reconfigurability is demonstrated using two designs. The first design employs a truncated patch antenna that emits circularly polarized radiation at 2.5 GHz. The antenna is placed on a Rogers 5880 duroid substrate with an acrylic substrate underneath to contain the LM channels. Using these channels, the circular polarization is converted to linear with a 15 dB difference between cross and co-polarized gain. Both antenna states show good matching and gain while maintaining

the same operational frequency. The second design has the same substrate stackup with a double truncated patch and a second channel underneath it. Using the two channels independently, this antenna shows polarization agility with three different operating states, LP (vacuum channel), RHCP (channel 1) and LHCP (channel 2). The antenna is well matched and shows adequate gain while switching between these states.

CHAPTER 5: CONCLUSION

5.1 Conclusions

The flow of LM through microfluid channels has emerged as a novel method for achieving reconfiguration within antenna systems. The insertion and removal of EGaIn has shown to achieve different types of reconfigurability. This thesis presents three different designs that achieve reconfiguration with using EGaIn that is integrated with an acrylic substrate. The first design employs a circular patch antenna that uses a frequency switchable AMC surface. The microfluid channel is designed in tandem with the AMC to enhance the gain for both frequencies. Thus, the design can achieve two distinct operating states, 2.48 GHz with a gain of 7.5 dBi with a vacuum channel and 1.65 GHz with a gain of 4 dBi with a EGaIn channel. The second design use a truncated patch antenna that can alter its current to radiate with linear or right-hand circular polarized radiation. A concise design procedure for the shape and placement of the LM channels to achieve optimal functioning is developed. This procedure is then employed to design a frequency agile antenna system that can freely switch between linear, left- and right-hand circular polarizations at 2.5 GHz. The antenna has strategically placed LM channels that produce 3 operating states effectively demonstrating polarization reconfigurability.

5.2 Future Work

The use of LM is an emerging field, and a matured fabrication process is yet to be developed. The fabrication methodology employed by different researchers are design specific and the challenges faced within fabrication are yet to be fully explored. Hence, the next step is to fabricate a physical prototype of the simulated designs. The realization

of the antenna and metallic layers can be done through a well refined PCB process. The microfluidic channels on the other hand can be realized in a few different methods. The planned fabrication procedure will use lasers to engrave the channel into the acrylic substrate and the selection of the acrylic reflects this requirement. However, the accuracy of the engraving process presents the first challenge. Unexpected variations in the laser's movement could result in the dimensions or positioning of the channels to change. While simulations can account for this by adding larger margins, a significant deviation can still result in a completely different radiation performance.

Furthermore, the simulations present a basis to achieve reconfiguration and verifying their operation through a prototype is essentially. The design's impedance and radiation performance will need to be measured, and the method of reconfiguration presents the second challenge. Since these designs switch their states through the flow of EGaIn, the prototype be disturbed to insert or remove the LM. The EGaIn is moved through the design with the help of syringes that are located at the beginning and end of the channels. The acrylic substrate from the simulation is modified to ensure that these syringes are placed far away from the antenna and the LM can be safely injected. The acrylic is extended on either side to allow a longer channel, and this prototype will ensure the functionality seen in the simulations are practically achievable.

The challenges described are attributed to the novelty of microfluidic channels. The fabrication of these designs will help in developing a methodology that can be used to enhance the available literature. Furthermore, the designs presented in this thesis add to a few designs using LM to achieve antenna reconfiguration.

BIBLIOGRAPHY

[1] C. A. Balanis, *Antenna Theory: Analysis and Design*, 2nd ed., no. 08. John Wiley & Sons, Inc., 1938.

[2] Vinaya. Y. Deshmukh and S. S. Chorage, “Review of Reconfigurable Antennas for Future Wireless Communication,” in *2020 International Conference on Emerging Smart Computing and Informatics (ESCI)*, IEEE, Mar. 2020, pp. 28–33. doi: 10.1109/ESCI48226.2020.9167528.

[3] V. Suryapaga and V. V. Khairnar, “Review on Multifunctional Pattern and Polarization Reconfigurable Antennas,” *IEEE Access*, vol. 12, pp. 90218–90251, 2024, doi: 10.1109/ACCESS.2024.3420426.

[4] S. Yang, Y. Chen, C. Yu, Y. Gong, and F. Tong, “Design of a Low-Profile, Frequency- Reconfigurable, and High Gain Antenna Using a Varactor-Loaded AMC Ground,” *IEEE Access*, vol. 8, pp. 158635–158646, 2020, doi: 10.1109/ACCESS.2020.3020853.

[5] Y. Tawk, J. Costantine, and C. G. Christodoulou, “A Varactor-Based Reconfigurable Filtenna,” *IEEE Antennas Wirel Propag Lett*, vol. 11, pp. 716–719, 2012, doi: 10.1109/LAWP.2012.2204850.

[6] Z. Mahlaoui, E. Antonino-Daviu, M. Ferrando-Bataller, H. Benchakroun, and A. Latif, “Frequency reconfigurable patch antenna with defected ground structure using varactor diodes,” in *2017 11th European Conference on Antennas and Propagation (EUCAP)*, IEEE, Mar. 2017, pp. 2217–2220. doi: 10.23919/EuCAP.2017.7928358.

[7] M. Riel and J.-J. Laurin, “Design of an Electronically Beam Scanning Reflectarray Using Aperture-Coupled Elements,” *IEEE Trans Antennas Propag*, vol. 55, no. 5, pp. 1260–1266, May 2007, doi: 10.1109/TAP.2007.895586.

[8] F. Venneri, S. Costanzo, and G. Di Massa, “Design and Validation of a Reconfigurable Single Varactor-Tuned Reflectarray,” *IEEE Trans Antennas Propag*, vol. 61, no. 2, pp. 635–645, Feb. 2013, doi: 10.1109/TAP.2012.2226229.

[9] Q. Chen, J. Ala-Laurinaho, A. Khripkov, J. Ilvonen, R. M. Moreno, and V. Viikari, “Varactor-Based Frequency-Reconfigurable Dual-Polarized mm-Wave Antenna Array for Mobile Devices,” *IEEE Trans Antennas Propag*, vol. 71, no. 8, pp. 6628–6638, Aug. 2023, doi: 10.1109/TAP.2023.3287679.

[10] M. Ikram, N. Nguyen-Trong, and A. Abbosh, “A Simple Single-Layered Continuous Frequency and Polarization-Reconfigurable Patch Antenna Array,” *IEEE Trans Antennas Propag*, vol. 68, no. 6, pp. 4991–4996, Jun. 2020, doi: 10.1109/TAP.2019.2952461.

[11] T. J. Jung, I.-J. Hyeon, C.-W. Baek, and S. Lim, “Circular/Linear Polarization Reconfigurable Antenna on Simplified RF-MEMS Packaging Platform in K-Band,”

IEEE Trans Antennas Propag, vol. 60, no. 11, pp. 5039–5045, Nov. 2012, doi: 10.1109/TAP.2012.2207662.

[12] A. Grau, J. Romeu, Ming-Jer Lee, S. Blanch, L. Jofre, and F. De Flaviis, “A Dual-Linearly-Polarized MEMS-Reconfigurable Antenna for Narrowband MIMO Communication Systems,” *IEEE Trans Antennas Propag*, vol. 58, no. 1, pp. 4–17, Jan. 2010, doi: 10.1109/TAP.2009.2036197.

[13] M. Al-Omari, H. Attia, K. K. Qureshi, and S. I. M. Sheikh, “Design of Frequency-Reconfigurable Antenna on Dielectric and Magnetic Metamaterial Composite Substrate,” *IEEE Antennas Wirel Propag Lett*, vol. 22, no. 4, pp. 943–947, Apr. 2023, doi: 10.1109/LAWP.2022.3230827.

[14] F. A. Ghaffar, M. Vaseem, L. Roy, and A. Shamim, “Design and Fabrication of a Frequency and Polarization Reconfigurable Microwave Antenna on a Printed Partially Magnetized Ferrite Substrate,” *IEEE Trans Antennas Propag*, vol. 66, no. 9, pp. 4866–4871, Sep. 2018, doi: 10.1109/TAP.2018.2846796.

[15] M. A. Amiri, C. A. Balanis, and C. R. Birtcher, “Gain and Bandwidth Enhancement of Ferrite-Loaded CBS Antenna Using Material Shaping and Positioning,” *IEEE Antennas Wirel Propag Lett*, vol. 12, pp. 611–614, 2013, doi: 10.1109/LAWP.2013.2260519.

[16] T. Wang, H. Zhai, J. Li, and Q. Sun, “Ferrite-Loaded Magnetically Reconfigurable SIW Magnetic Dipole Antenna With Tunable Frequencies,” *IEEE Antennas Wirel Propag Lett*, vol. 23, no. 10, pp. 2969–2973, Oct. 2024, doi: 10.1109/LAWP.2024.3416521.

[17] K. N. Paracha, A. D. Butt, A. S. Alghamdi, S. A. Babale, and P. J. Soh, “Liquid Metal Antennas: Materials, Fabrication and Applications,” *Sensors*, vol. 20, no. 1, p. 177, Dec. 2019, doi: 10.3390/s20010177.

[18] M. D. Dickey, R. C. Chiechi, R. J. Larsen, E. A. Weiss, D. A. Weitz, and G. M. Whitesides, “Eutectic Gallium-Indium (EGaIn): A Liquid Metal Alloy for the Formation of Stable Structures in Microchannels at Room Temperature,” *Adv Funct Mater*, vol. 18, no. 7, pp. 1097–1104, Apr. 2008, doi: 10.1002/adfm.200701216.

[19] M. Wang, M. R. Khan, M. D. Dickey, and J. J. Adams, “A Compound Frequency- and Polarization- Reconfigurable Crossed Dipole Using Multidirectional Spreading of Liquid Metal,” *IEEE Antennas Wirel Propag Lett*, vol. 16, pp. 79–82, 2017, doi: 10.1109/LAWP.2016.2556983.

[20] X. Bai, M. Su, Y. Liu, and Y. Wu, “Wideband Pattern-Reconfigurable Cone Antenna Employing Liquid-Metal Reflectors,” *IEEE Antennas Wirel Propag Lett*, vol. 17, no. 5, pp. 916–919, May 2018, doi: 10.1109/LAWP.2018.2823301.

[21] C. Wang, J. C. Yeo, H. Chu, C. T. Lim, and Y.-X. Guo, “Design of a Reconfigurable Patch Antenna Using the Movement of Liquid Metal,” *IEEE Antennas Wirel Propag Lett*, vol. 17, no. 6, pp. 974–977, Jun. 2018, doi: 10.1109/LAWP.2018.2827404.

[22] L. Song, W. Gao, C. O. Chui, and Y. Rahmat-Samii, “Wideband Frequency Reconfigurable Patch Antenna With Switchable Slots Based on Liquid Metal and 3-D Printed Microfluidics,” *IEEE Trans Antennas Propag*, vol. 67, no. 5, pp. 2886–2895, May 2019, doi: 10.1109/TAP.2019.2902651.

[23] Y. Liu, Q. Wang, Y. Jia, and P. Zhu, “A Frequency- and Polarization-Reconfigurable Slot Antenna Using Liquid Metal,” *IEEE Trans Antennas Propag*, vol. 68, no. 11, pp. 7630–7635, Nov. 2020, doi: 10.1109/TAP.2020.2993110.

[24] J. Hao, J. Ren, X. Du, J. H. Mikkelsen, M. Shen, and Y. Z. Yin, “Pattern-Reconfigurable Yagi–Uda Antenna Based on Liquid Metal,” *IEEE Antennas Wirel Propag Lett*, vol. 20, no. 4, pp. 587–591, Apr. 2021, doi: 10.1109/LAWP.2021.3058115.

[25] L. Song, W. Gao, and Y. Rahmat-Samii, “3-D Printed Microfluidics Channelizing Liquid Metal for Multipolarization Reconfigurable Extended E-Shaped Patch Antenna,” *IEEE Trans Antennas Propag*, vol. 68, no. 10, pp. 6867–6878, Oct. 2020, doi: 10.1109/TAP.2020.2993079.

[26] W. Zhu, X. Liu, Y. Fan, Z. Zhang, and X. Ma, “Transparent and Flexible Antenna With Polarization Reconfigurability Using EGaIn for Wearable Applications,” *IEEE Trans Antennas Propag*, vol. 72, no. 10, pp. 7493–7503, Oct. 2024, doi: 10.1109/TAP.2024.3439882.

[27] O. M. Sanusi, Y. Wang, and L. Roy, “Reconfigurable Polarization Converter Using Liquid Metal Based Metasurface,” *IEEE Trans Antennas Propag*, vol. 70, no. 4, pp. 2801–2810, Apr. 2022, doi: 10.1109/TAP.2021.3137217.

[28] V. Sharbati, X. Bao, J. J. Healy, N. Zhang, K. Nadali, and M. J. Ammann, “Dynamic Tuning of Notch Bands in UWB Antenna Based on Liquid Metal for Cognitive Radio Applications,” *IEEE Antennas Wirel Propag Lett*, vol. 23, no. 12, pp. 4708–4712, Dec. 2024, doi: 10.1109/LAWP.2024.3466613.

[29] Y. Liu, Z. Liu, Q. Wang, and Y. Jia, “Low-RCS Antenna Array With Switchable Scattering Patterns Employing Microfluidic Liquid Metal Alloy-Based Metasurface,” *IEEE Trans Antennas Propag*, vol. 69, no. 12, pp. 8955–8960, Dec. 2021, doi: 10.1109/TAP.2021.3090510.

[30] X.-F. Li, Y.-L. Ban, Q. Sun, Y.-X. Che, and J. Hu, “Compact Dual-Frequency 2-D Van Atta Array Using the Reconfigurable AMC Antenna,” *IEEE Antennas Wirel Propag Lett*, vol. 22, no. 12, pp. 3162–3166, Dec. 2023, doi: 10.1109/LAWP.2023.3312417.

[31] Y.-F. Cheng, J. Feng, C. Liao, and X. Ding, “Analysis and Design of Wideband Low-RCS Wide-Scan Phased Array With AMC Ground,” *IEEE Antennas Wirel Propag Lett*, vol. 20, no. 2, pp. 209–213, Feb. 2021, doi: 10.1109/LAWP.2020.3044533.

[32] H. Malekpoor and S. Jam, “Improved Radiation Performance of Low Profile Printed Slot Antenna Using Wideband Planar AMC Surface,” *IEEE Trans Antennas Propag*, vol. 64, no. 11, pp. 4626–4638, Nov. 2016, doi: 10.1109/TAP.2016.2607761.